ENGINEERING OF BIOMATERIALS

INŻYNIERIA BIOMATERIAŁÓW

JOURNAL OF POLISH SOCIETY FOR BIOMATERIALS AND FACULTY OF MATERIALS SCIENCE AND CERAMICS AGH-UST
CZASOPISMO POLSKIEGO STOWARZYSZENIA BIOMATERIAŁÓW I WYDZIAŁU INŻYNIERII MATERIAŁOWEJ I CERAMIKI AGH

Number 147
Numer 147
Volume XXI
Rok XXI

OCTOBER 2018
PAŹDZIERNIK 2018

ISSN 1429-7248

PUBLISHER:
WYDAWCA:

Polish Society for Biomaterials in Krakow
Polskie Stowarzyszenie Biomateriałów w Krakowie

ADDRESS OF EDITORIAL OFFICE:
ADRES REDAKCJI:

AGH-UST
30/A3, Mickiewicz Av.
30-059 Krakow, Poland
Akademia Górniczo-Hutnicza
al. Mickiewicza 30/A-3
30-059 Kraków

Issue: 250 copies
Nakład: 250 egz.

Scientific Publishing House AKAPIT
Wydawnictwo Naukowe AKAPIT
e-mail: wn@akapit.krakow.pl

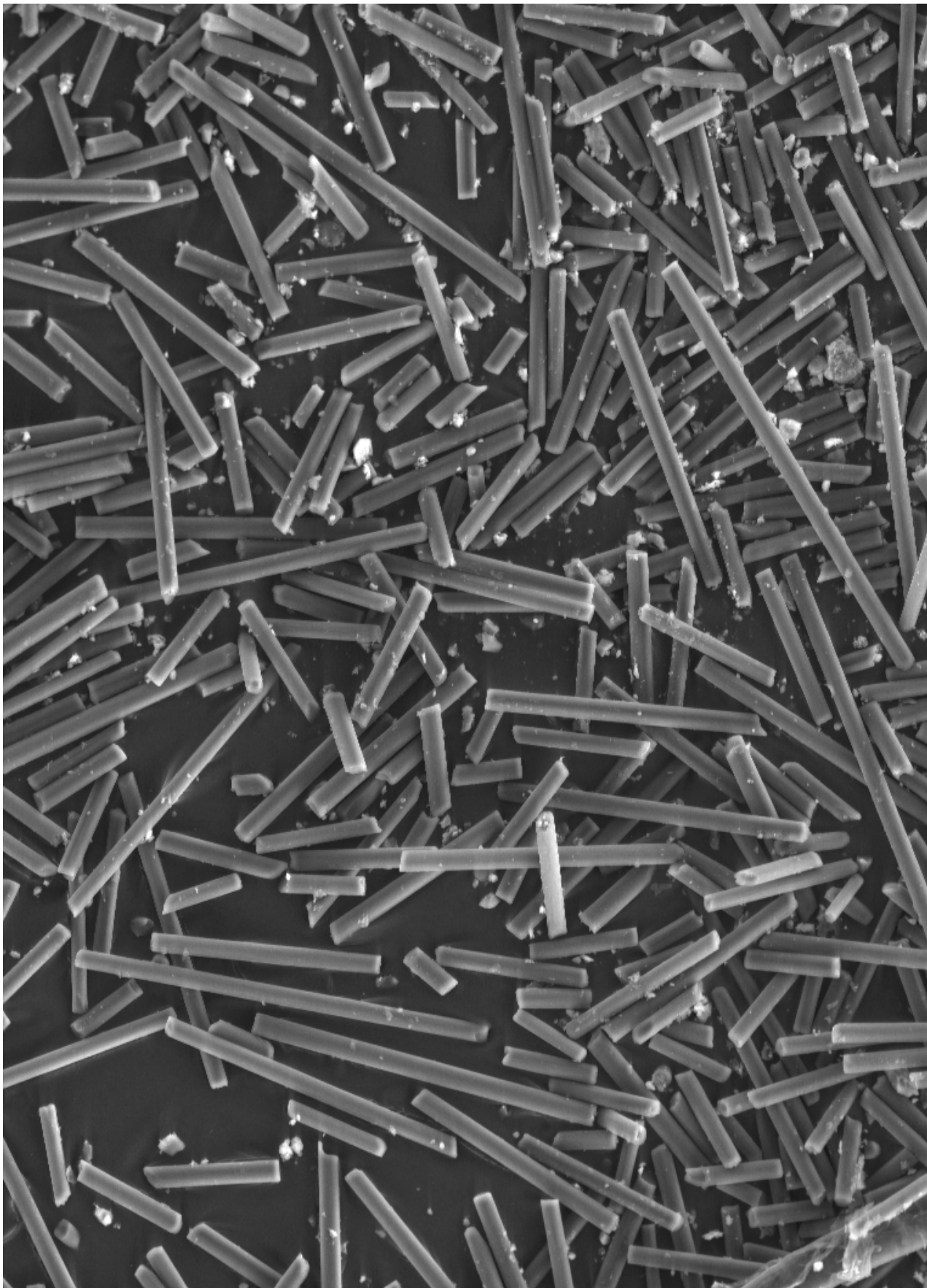

ENGINEERING OF BIOMATERIALS

EDITORIAL BOARD
KOMITET REDAKCYJNY

INTERNATIONAL EDITORIAL BOARD
MIĘDZYNARODOWY KOMITET REDAKCYJNY

ENGINEERING OF BIOMATERIALS

Wskazówki dla autorów

1. Prace do opublikowania w kwartalniku „Engineering of Biomaterials / Inżynieria Biomateriałów" przyjmowane będą wyłącznie w języku angielskim. Możliwe jest również dołączenie dodatkowo polskiej wersji językowej.
2. Wszystkie nadsyłane artykuły są recenzowane.
3. Materiały do druku prosimy przysyłać na adres e-mail: kabe@agh.edu.pl.
4. Struktura artykułu:
• TYTUŁ • Autorzy i instytucje • Streszczenie (200-250 słów) • Słowa kluczowe (4-6) • Wprowadzenie • Materiały i metody • Wyniki i dyskusja • Wnioski • Podziękowania • Piśmiennictwo
5. Autorzy przesyłają pełną wersję artykułu, łącznie z ilustracjami, tabelami, podpisami i literaturą w jednym pliku. Artykuł w tej formie przesyłany jest do recenzentów. Dodatkowo autorzy proszeni są o przesłanie materiałów ilustracyjnych (rysunki, schematy, fotografie, wykresy) w oddzielnych plikach (format np. .jpg, .gif., .tiff, .bmp). Rozdzielczość rysunków min. 300 dpi. Wszystkie rysunki i wykresy powinny być czarno-białe lub w odcieniach szarości i ponumerowane cyframi arabskimi. W tekście należy umieścić odnośniki do rysunków i tabel. W przypadku artykułów dwujęzycznych w tabelach i na wykresach należy umieścić opisy polskie i angielskie.
6. Na końcu artykułu należy podać wykaz piśmiennictwa w kolejności cytowania w tekście i kolejno ponumerowany.
7. Redakcja zastrzega sobie prawo wprowadzenia do opracowań autorskich zmian terminologicznych, poprawek redakcyjnych, stylistycznych, w celu dostosowania artykułu do norm przyjętych w naszym czasopiśmie. Zmiany i uzupełnienia merytoryczne będą dokonywane w uzgodnieniu z autorem.
8. Opinia lub uwagi recenzentów będą przekazywane Autorowi do ustosunkowania się. Nie dostarczenie poprawionego artykułu w terminie oznacza rezygnację Autora z publikacji pracy w naszym czasopiśmie.
9. Za publikację artykułów redakcja nie płaci honorarium autorskiego.
10. Adres redakcji:

Czasopismo
„Engineering of Biomaterials / Inżynieria Biomateriałów"
Akademia Górniczo-Hutnicza im. St. Staszica
Wydział Inżynierii Materiałowej i Ceramiki
al. Mickiewicza 30/A-3, 30-059 Kraków
tel. (48) 12 617 25 03, 12 617 25 61
tel./fax: (48) 12 617 45 41
e-mail: chlopek@agh.edu.pl, kabe@agh.edu.pl

Szczegółowe informacje dotyczące przygotowania manuskryptu oraz procedury recenzowania dostępne są na stronie internetowej czasopisma:
www.biomat.krakow.pl

Warunki prenumeraty

Zamówienie na prenumeratę prosimy przesyłać na adres:
mgr inż. Augustyn Powroźnik
apowroz@agh.edu.pl, tel/fax: (48) 12 617 45 41
Cena pojedynczego numeru wynosi 20 PLN
Konto: Polskie Stowarzyszenie Biomateriałów
30-059 Kraków, al. Mickiewicza 30/A-3
ING Bank Śląski S.A. O/Kraków
nr rachunku 63 1050 1445 1000 0012 0085 6001

Prenumerata obejmuje 4 numery regularne i nie obejmuje numeru specjalnego (materiały konferencyjne).

Instructions for authors

1. Papers for publication in quarterly journal „Engineering of Biomaterials / Inżynieria Biomateriałów" should be written in English.
2. All articles are reviewed.
3. Manuscripts should be submitted to editorial office by e-mail to kabe@agh.edu.pl.
4. A manuscript should be organized in the following order:
• TITLE • Authors and affiliations • Abstract (200-250 words) • Keywords (4-6) • Introduction • Materials and Methods • Results and Discussions • Conclusions • Acknowledgements • References
5. All illustrations, figures, tables, graphs etc. preferably in black and white or grey scale should be additionally sent as separate electronic files (format .jpg, .gif., .tiff, .bmp). High-resolution figures are required for publication, at least 300 dpi. All figures must be numbered in the order in which they appear in the paper and captioned below. They should be referenced in the text. The captions of all figures should be submitted on a separate sheet.
6. References should be listed at the end of the article. Number the references consecutively in the order in which they are first mentioned in the text.
7. The Editors reserve the right to improve manuscripts on grammar and style and to modify the manuscripts to fit in with the style of the journal. If extensive alterations are required, the manuscript will be returned to the authors for revision.
8. Opinion or notes of reviewers will be transferred to the author. If the corrected article will not be supplied on time, it means that the author has resigned from publication of work in our journal.
9. Editorial does not pay author honorarium for publication of article.
10. Address of editorial office:

Journal
„Engineering of Biomaterials / Inżynieria Biomateriałów"
AGH University of Science and Technology
Faculty of Materials Science and Ceramics
30/A-3, Mickiewicz Av., 30-059 Krakow, Poland
tel. (48) 12) 617 25 03, 12 617 25 61
tel./fax: (48) 12 617 45 41
e-mail: chlopek@agh.edu.pl, kabe@agh.edu.pl

Detailed information concerning manuscript preparation and review process are available at the journal's website:
www.biomat.krakow.pl

Subscription terms

Contact:
MSc Augustyn Powroźnik,
e-mail: apowroz@agh.edu.pl
Subscription rates:
Cost of one number: 20 PLN
Payment should be made to:
Polish Society for Biomaterials
30/A3, Mickiewicz Av.
30-059 Krakow, Poland
ING Bank Slaski S.A.
account no. 63 1050 1445 1000 0012 0085 6001

Subscription includes 4 issues and does not include special issue (conference materials).

28th Biomaterials in Medicine and Veterinary Medicine

Annual Conference

10 – 13 October 2019 Rytro, Poland

SAVE THE DATE

10-13

OCTOBER

2019

www.biomat.agh.edu.pl

REGISTER

AND

SUBMIT

AN ABSTRACT

STUDIA PODYPLOMOWE
Biomateriały – Materiały dla Medycyny
2019/2020

Organizator: Akademia Górniczo-Hutnicza im. Stanisława Staszica w Krakowie Wydział Inżynierii Materiałowej i Ceramiki Katedra Biomateriałów i Kompozytów **Kierownik:** prof. dr hab. inż. Elżbieta Pamuła **Sekretarz:** dr inż. Małgorzata Krok-Borkowicz	**Adres:** 30-059 Kraków, Al. Mickiewicza 30 Pawilon A3, p. 208, 210 lub 501 tel. 12 617 44 48, 12 617 23 38, fax. 12 617 33 71 email: epamula@agh.edu.pl; krok@agh.edu.pl http://www.agh.edu.pl/ksztalcenie/oferta-ksztalcenia/studia-podyplomowe/biomaterialy-materialy-dla-medycyny/

Charakterystyka:
Tematyka prezentowana w trakcie zajęć obejmuje przegląd wszystkich grup materiałów dla zastosowań medycznych: metalicznych, ceramicznych, polimerowych, węglowych i kompozytowych. Słuchacze zapoznają się z metodami projektowania i wytwarzania biomateriałów a następnie możliwościami analizy ich właściwości mechanicznych, właściwości fizykochemicznych (laboratoria z metod badań: elektronowa mikroskopia skaningowa, mikroskopia sił atomowych, spektroskopia w podczerwieni, badania energii powierzchniowej i zwilżalności) i właściwości biologicznych (badania: *in vitro* i *in vivo*). Omawiane są regulacje prawne i aspekty etyczne związane z badaniami na zwierzętach i badaniami klinicznymi (norma EU ISO 10993). Słuchacze zapoznają się z najnowszymi osiągnięciami w zakresie nowoczesnych nośników leków, medycyny regeneracyjnej i inżynierii tkankowej.

Sylwetka absolwenta:
Studia adresowane są do absolwentów uczelni technicznych (inżynieria materiałowa, technologia chemiczna), przyrodniczych (chemia, biologia, biotechnologia) a także medycznych, stomatologicznych, farmaceutycznych i weterynaryjnych, pragnących zdobyć, poszerzyć i ugruntować wiedzę z zakresu inżynierii biomateriałów i nowoczesnych materiałów dla medycyny. Słuchacze zdobywają i/lub pogłębiają wiedzę z zakresu inżynierii biomateriałów. Po zakończeniu studiów wykazują się znajomością budowy, właściwości i sposobu otrzymywania materiałów przeznaczonych dla medycyny. Potrafią analizować wyniki badań i przekładać je na zachowanie się biomateriału w warunkach żywego organizmu. Ponadto słuchacze wprowadzani są w zagadnienia dotyczące wymagań normowych, etycznych i prawnych niezbędnych do wprowadzenia nowego materiału na rynek. Ukończenie studiów pozwala na nabycie umiejętności przygotowywania wniosków do Komisji Etycznych i doboru metod badawczych w zakresie analizy biozgodności materiałów.

Zasady naboru:
Termin zgłoszeń: od 20.09.2019 do 20.10.2019 (liczba miejsc ograniczona - decyduje kolejność zgłoszeń)
Wymagane dokumenty: dyplom ukończenia szkoły wyższej
Osoby przyjmujące zgłoszenia:
prof. dr hab. inż. Elżbieta Pamuła (pawilon A3, p. 208, tel. 12 617 44 48, e-mail: epamula@agh.edu.pl)
dr inż. Małgorzata Krok-Borkowicz (pawilon A3, p. 210, tel. 12 617 23 38, e-mail: krok@agh.edu.pl)

Czas trwania: 2 semestry (od XI 2019 r. do VI 2020 r.) 8 zjazdów (soboty-niedziele) 1 raz w miesiącu	**Opłaty:** 2 600 zł

SPIS TREŚCI
CONTENTS

Wersja papierowa czasopisma „Engineering of Biomaterials / Inżynieria Biomateriałów" jest jego wersją pierwotną
Printed version of „Engineering of Biomaterials / Inżynieria Biomateriałów" is a primary version of the journal

PREPARATION OF PSYLLIUM HUSK POWDER BASED MICROPOROUS COMPOSITE SCAFFOLDS FOR TISSUE ENGINEERING

Suruchi Poddar, Piyush Sunil Agarwal, Sanjeev Kumar Mahto*

Tissue Engineering and Biomicrofluidics Laboratory,
School of Biomedical Engineering,
Indian Institute of Technology,
Banaras Hindu University, Varanasi, India
*e-mail: skmahto.bme@iitbhu.ac.in

Abstract

This study demonstrates the comparison in the method of fabrication and thus evaluates the potential of psyllium husk powder and gelatin-based composite microporous scaffolds for tissue engineering applications. The scaffold is being prepared in three different ratios of 50:50, 75:25 and 100 (w/w of psyllium husk powder and gelatin, respectively) by employing a suitable cross-linking agent, EDC-NHS, followed drying. We have demonstrated the use and outcomes of two different methods of scaffold drying, i.e., vacuum desiccation along with liquid nitrogen dip and lyophilization. It was concluded from the SEM micrographs that the scaffolds dried under vacuum accompanied with liquid nitrogen exposure exhibited less porous architecture when compared to those prepared using a lyophilizer, that resulted in pores in the range of 60-110 µm. Scaffolds fabricated using the former technique lost porosity and sponge-like characteristics of a scaffold. In spite of the above fact, water retaining capacity and stability in the cell culture of such scaffolds is significant, nearly 40-50% of its initial dry weight. Cell culture experiments support the potential of the scaffolds prepared from different methods of fabrication for its cytocompatibility and suitability for cell growth and proliferation for a substantial duration. Erosion in the porous design of the scaffolds was observed after 14 days via SEM micrographs. It was inferred that freeze-drying is a better technique than vacuum desiccation for scaffold preparation. The present investigation has been conducted keeping in mind the importance of drying a scaffold. Scaffold drying is a necessary step to increase its shelf-life, makes it easy to transport and much importantly, controlling the pore size of the scaffold.

Keywords: *Psyllium husk powder, EDC-NHS coupling reaction, microporous scaffolds, hydrogel, freeze--drying, vacuum desiccation*

[Engineering of Biomaterials 147 (2018) 2-6]

Introduction

Tissue engineering is a mixed discipline that mainly focuses on the recreation and regeneration of diseased or damaged tissues [1,2]. Design and development of microporous three-dimensional scaffolds are one of the potential domain of research for tissue engineering and regenerative medicine. Scaffolds form an integral part of tissue engineering as they allow us to mimic native tissue-like environment by complying the structural, biological and mechanical attributes of the extracellular matrix (ECM) present in the native tissues [3]. Very briefly, scaffolds provide an anatomical framework for the cells to reside, the porosity of the scaffold supports metabolite transport efficiently, the strength of the scaffolds is responsible for the mechanical characteristics of the cells, facilitates cell growth and proliferation by providing them enough cues to respond and communicate amongst each other. Therefore, tissue engineering scaffolds are an absolute necessity that provides a conducive environment for cell growth and reproduction with respect to its three-dimensional structure, pore size, strength, cell attachment, degradation rate, etc. [4,5].

Although researchers have access to a plethora of available biomaterials from synthetic such as poly(vinyl alcohol) (PVA), polycaprolactone (PCL), poly (glycolic acid) (PGA), to natural such as cellulose, alginate, gelatin, chitosan, etc., natural biomaterials are particularly being selected for their easy availability, low toxicity, enhanced bioactivity and cytocompatibility [6,7]. With the advancement in tissue engineering the use of plant-derived biopolymers such as alginate, guar gum, aloe gel to name a few, have gained momentum. Easy accessibility, high acceptability and their use in the treatment of human ailments over many decades have made them the material of choice for tissue engineering applications. Plantago ovata or psyllium husk is one of the most widely used and commercially available plant-derived polysaccharides in Indian markets [8]. It has been used in many biomedical applications because of its ease of availability, low cost, non-toxicity, biodegradability, and safety [9]. Gelatin, a versatile and naturally occurring biopolymer helps in the modulation of cell adhesion because of the presence of cell adhering moieties [10-15]. It has been used as an acceptable scaffolding biomaterial for cardiac, hepatic, skin, bone and many such tissue engineering applications [16].1-ethyl-3-(3-dimethylaminopropyl)-1-carbodiimide hydrochloride (EDC) and N-hydroxysuccinimide (NHS) has been used as a cross-linking agent as it introduces an amide or an ester bond between the functional moieties of the biopolymers [17-19]. The use of EDC-NHS does not involve any addition of spacer arms between the conjugating molecules as it belongs to a class of zero-length cross-linker [20]. This unique feature of EDC-NHS makes it a potential cross-linker as it does not integrate with the final product and leaves no toxic substance in the fabricated scaffold [21,22].

Scaffold drying is an important step for scaffold preparation. It increases the shelf-life of the material and thus the scaffold, makes it easier to transport, allows a control over the range of pore sizes formed within the scaffold which is a critical feature for cell growth, provides a uniform structure and maintains the integrity of the scaffold and to some extent provides an aesthetic value to the scaffolds [23]. Freeze-drying involves the use of present ice-crystals as a template for pore formation. It applies the principle of sublimation that occurs when the formed ice-crystals go directly to the gaseous state thus omitting the liquid phase. This process allows little control over pore size and interconnectivity between the pores is maintained and prevents the structure from collapsing [24,25].

The main aim of this study is to compare the drying methods of vacuum desiccation and freeze-drying in the fabrication and characterization of psyllium husk powder and gelatin-based three-dimensional microporous scaffolds, cross-linked with EDC-NHS coupling reaction, thus supporting its potential for tissue engineering applications.

Materials and Methods

Psyllium husk powder and gelatin (FIG. 1 a,b) composite scaffolds were prepared by mixing them in the three different ratios, namely 50:50, 75:25 and 100:0 (w/w) respectively, in water. A total of 0.4 g of psyllium was mixed with 14 mL of distilled water to prepare 100% psyllium husk scaffolds. Similarly, the ratios 50:50 and 75:25 were also prepared. The prepared ratios were then cross-linked using 25 mM EDC and 10 mM NHS solution prepared in 95% alcohol solution at an acidic pH, as already explained in detail elsewhere [26] followed by a drying step. Digital photographs of the fabricated scaffolds were captured from a 13-megapixel digital camera. In the present study, one set of scaffolds were dried for two days using a desiccator connected to a vacuum pump accompanied with a liquid nitrogen dip for 10-15 seconds for complete drying. The other set of scaffolds was cross-linked using the same procedure as above except it was dried for two days in a freeze-drier.

Scanning electron microscopy analysis using a Zeiss EVO 18 SEM (Zeiss, Oberkochen, Germany) at 20 kV, was carried out to determine the porous architecture of the scaffolds after respective drying steps. Cell culture studies were performed with L929-RFP (red fluorescent protein) mouse fibroblast cells to identify cell viability, growth, and cell-cell communication within the fabricated scaffold [27]. For freeze-dried scaffolds circular discs of the scaffolds were punched out with 5 mm diameter and similar thickness of the scaffolds was used, i.e. 1-2 mm approximately. Whereas for the scaffolds dried by vacuum desiccation and liquid nitrogen dip had become crispy and hard making it difficult to punch out discs of 5 mm diameter. Therefore, pieces of similar dimensions were cut and used for cell culture experiments. The scaffolds were sterilized by exposing them to ultra-violet radiation for 30 min inside a biosafety cabinet.

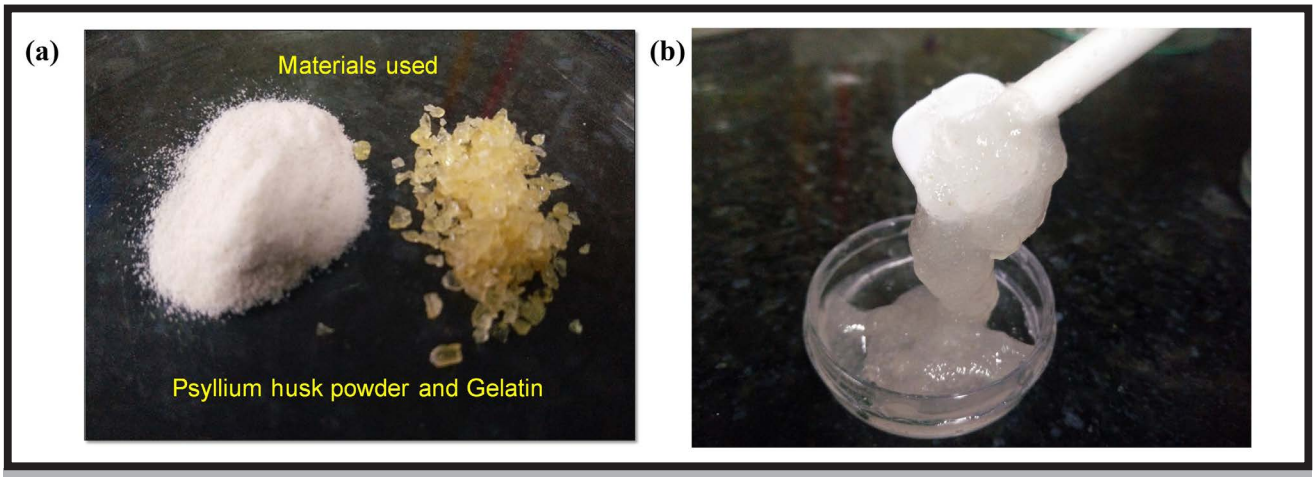

FIG. 1. Representative images of (a) raw materials, i.e. psyllium husk powder and gelatin, used in the fabrication of the scaffold and (b) the viscous mixture formed after mixing the raw materials.

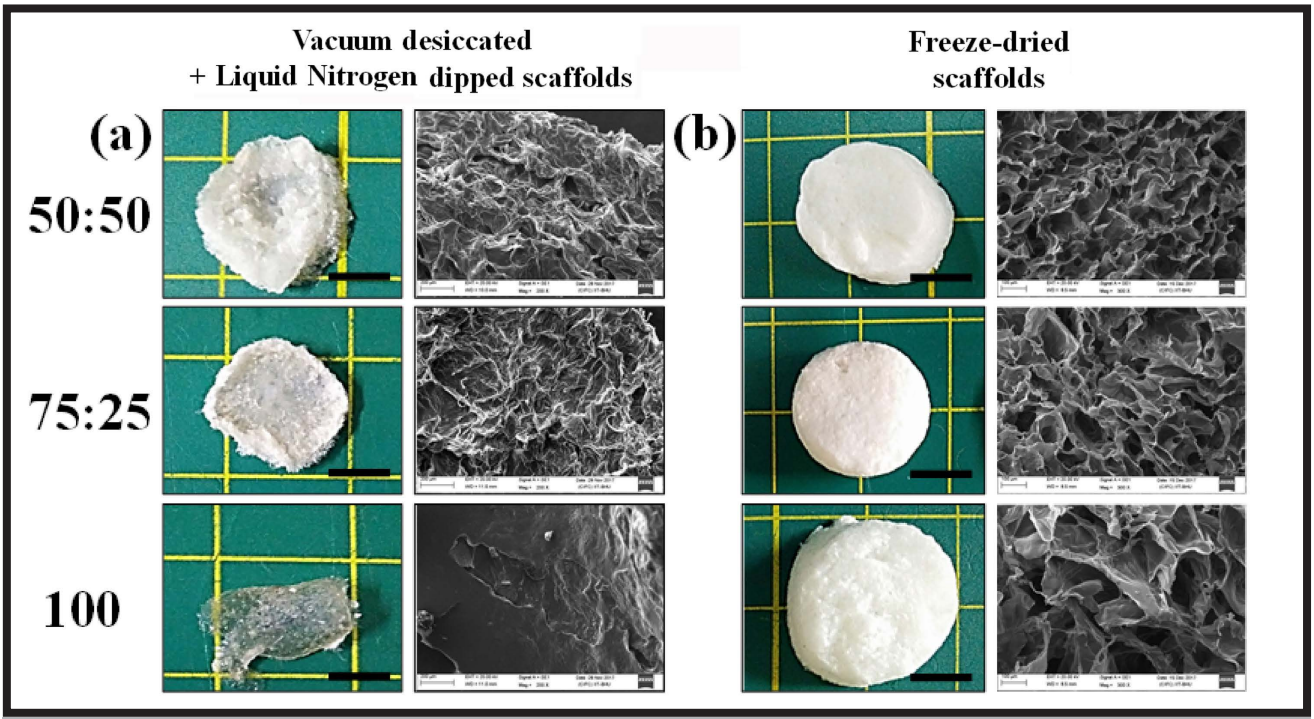

FIG. 2. Digital photographs of fabricated scaffolds by utilizing the two methods for drying the scaffolds and the SEM micrographs that depict porous architecture of the scaffolds. Scale bar: 0.5 cm.

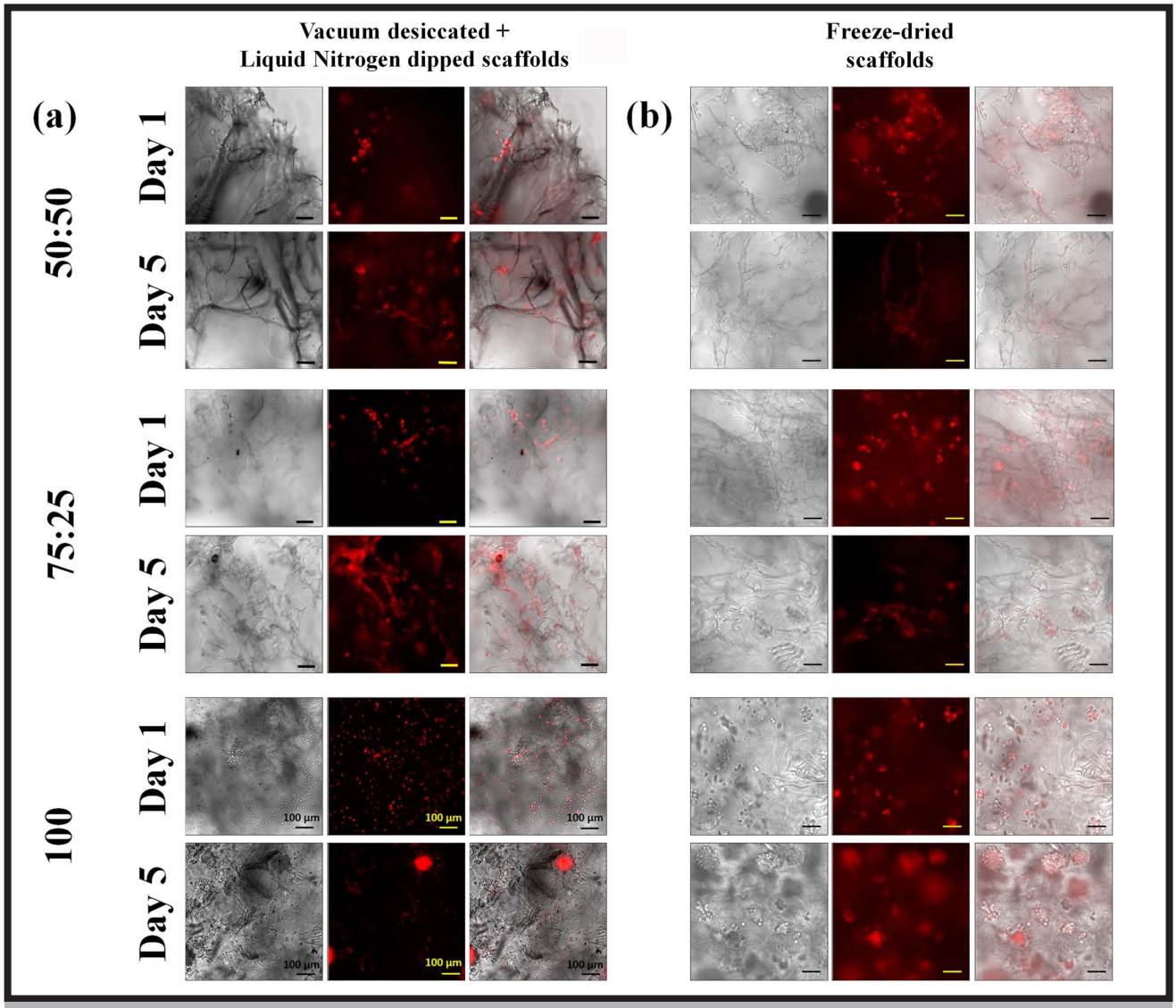

FIG. 3. Panel of images of L929-RFP mouse fibroblast cell culture within the scaffolds prepared from different drying techniques. The panels exhibit brightfield, fluorescent and merged images (from left-right) of the cells within the scaffolds at day 1 and day 5. Scale bar: 50 µm.

Cells were then seeded at a density of 10^5 cells per scaffold and the scaffolds were allowed to soak in the cell suspension solution for about half an hour inside a humidified CO_2 incubator (Galaxy® 170 S, Eppendorf, Germany). The scaffolds were placed in a Petri dish and fed with the optimum volume of cell culture medium that was maintained inside a humidified, 5% CO_2 incubator at 37°C for further experiment. The complete cell culture medium was prepared from Dulbecco's modified Eagle's Medium (DMEM, HiMedia), 10% fetal bovine serum (FBS, HiMedia) and 1% Penicillin/Streptomycin (HiMedia) antibiotic solution. The fluorescent images of L929-RFP cells within the scaffolds were collected at regular intervals using an inverted, DIC, fluorescence microscope (Nikon Ti-U).

Results and Discussions

It is observed from the digital photographs of the fabricated scaffolds that the first set of scaffolds, dried in a vacuum desiccator and exposed to liquid nitrogen, exhibits a contracted or deflated physical appearance (FIG. 2a) that seems to be progressing towards a sheet-like structure with pure psyllium (100) composition whereas the set of scaffolds subjected to freeze-drying protocol maintain the physical aspect and integrity of the scaffold (FIG. 2b). The polyhedral shape of the pores of the freeze-dried scaffolds spanned a range of 60-110 µm. The average pore size for all the three ratios of the scaffold was examined as 77 ± 24 µm. The difference in the physical attributes of the scaffolds prepared from two distinct procedures is due to the fact that vacuum desiccation followed by a dip in liquid nitrogen removed all the moisture from the scaffolds thereby leaving no void space within the scaffolds for it to be considered as microporous as highlighted from the SEM images (FIG. 2a). On the contrary, the freeze-drying procedure exploits water content as a template to create microporous structures within the scaffolds thus maintaining its porous morphology [28]. The basic principle of freeze-drying is the phenomenon of sublimation, that immediately converts solid into a vapour state without passing through a liquid state. The material to be dehydrated is first frozen and then subjected to a high vacuum. The complete procedure of lyophilization takes place at a low temperature and pressure that makes it an excellent method for preserving biological and heat-sensitive samples [29]. It was concluded from the cell culture images in FIG. 2 that scaffolds fabricated from both drying steps show equally good cell growth and proliferation when compared for a period of 5 days. The cellular proliferation was found to be >80% by the 6th day of cell culture in the fabricates scaffolds.

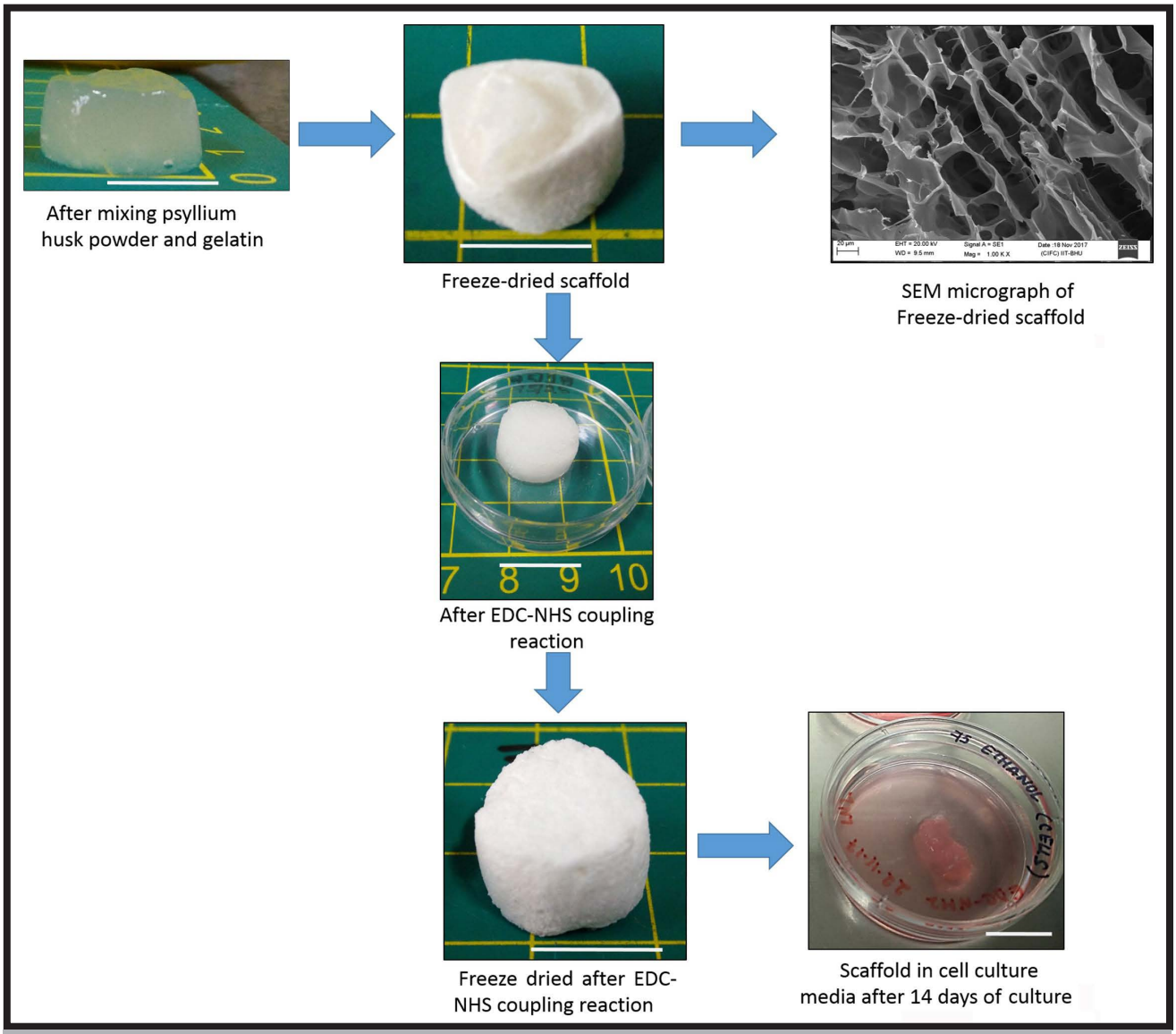

FIG. 4. Representative images of scaffolds at different stages of fabrication process as well as when incubated in culture medium. SEM image shows the internal geometry and microporous nature of the fabricated scaffolds. Scale bar: 1 cm.

The scaffolds dried by vacuum desiccation and liquid nitrogen show commendable swelling in their size when subjected to cell culture media. The reason behind this behaviour may be that while in a vacuum all the air was being sucked out of the scaffold leaving no void space behind which is clearly expressed from the SEM micrographs. Therefore, when a liquid medium was added, it readily absorbed all the solution inside it and distended like a balloon. The swelling capacity or the water imbibing ability of the fabricated scaffolds was investigated as 40-50% of its initial dry weight for scaffolds fabricated from both the techniques. The long-term in vitro degradation of the scaffolds till 14 days in physiological buffer (pH 7.4) at room temperature and at 37°C suggests its resistance towards hydrolytic degradation [30] that makes it a potential candidate for oral and subcutaneous drug delivery systems and tissue engineering applications. It is observed that by day 5 cells made immense network among themselves, a notable cell-cell communication and proliferation is also visible (FIG. 3 a,b). The cells were found to be present through-out the thickness of the scaffold when analysed from Z-stacking images revealing the porous architecture of the scaffolds. The scaffolds were appreciably stable in the cell culture media for a significantly long duration of 3-4 months, although cells were not visible within the scaffolds after 24 days. This indicates that though biodegradable in nature, the degradation of the scaffolds was slow because of its integrity obtained by cross-linking with EDC-NHS coupling reaction. With the given experimental conditions it was inferred that the ratio of 75:25 is most suitable for cell growth, differentiation, and proliferation. The sequence of steps followed in the fabrication process of scaffolds using EDC-NHS coupling reaction as a suitable cross-linker has been represented in FIG. 4.

Conclusions

The outcomes of the conducted study led us to the conclusion that EDC-NHS cross-linked scaffolds fabricated by freeze-drying step exhibit superior porous structure in comparison to those dried in a vacuum desiccator accompanied with liquid nitrogen dip. Although both sets of scaffolds were found suitable for cell growth and communication, structure and integrity of the scaffolds were better maintained in those developed using a freeze-drier, unlike the other set that presented a shrunken appearance. Therefore, in light of the above facts, it was inferred that scaffolds fabricated by the freeze-drying process were more suitable for cell culture and tissue engineering applications.

The fabricated scaffolds can be used in various tissue engineering and regenerative medicine applications such as wound dressing, sustained drug release, three-dimensional microporous scaffold for tissue regeneration and many more, based on the fact that: 1) they have remarkable water imbibing capacity of 40-50% of its initial dry weight, 2) enhanced mechanical strength, i.e. the crispy and brittle nature of the scaffolds obtained from the former technique was replaced by the strength to oppose crushing loads by freeze-drying. The cytocompatibility was determined to be ~80% for L929 fibroblast cells, which also projects its suitability for cell culture. The biodegradable nature of the fabricated scaffold makes it an acceptable platform for the development of bioengineered tissues. Moreover, such an economic type of natural biomaterials are easy to manufacture with minimal toxicity and worldwide acceptance.

Acknowledgments

This work was financially supported by a DST-INSPIRE (DST/INSPIRE/04/2013/000836) research grant from the Department of Science and Technology, Government of India. The authors would also like to thank the Institute Research Project (IRP) scheme for individual faculty provided by the Indian Institute of Technology (Banaras Hindu University) for the development of state-of-the-art facilities.

References

[1] V.R. Hokmabad, S. Davaran, A. Ramazani, R. Salehi: Design and fabrication of porous biodegradable scaffolds: a strategy for tissue engineering. Journal of Biomaterials Science, Polymer Edition 28(16) (2017) 1797-1825.
[2] P. Zhao, H. Gu, H. Mi, C. Rao, J. Fu, L. Turng: Fabrication of scaffolds in tissue engineering: A review. Front. Mech. Eng. 13(1) (2018) 107-119.
[3] B.P. Chan, K.W. Leong: Scaffolding in tissue engineering: general approaches and tissue-specific considerations. Eur Spine J 17(4) (2008) 467-479.
[4] F.J. O'Brien: Biomaterials & scaffolds for tissue engineering. Materials Today 14(3) (2011) 88-95.
[5] H. Zhang, L. Zhou, W. Zhang: Control of Scaffold Degradation in Tissue Engineering: A Review. Tissue Engineering Part B: Reviews 20(5) (2014) 492-502.
[6] E. Carletti, A. Motta, C. Migliaresi: Scaffolds for tissue engineering and 3D cell culture. Methods Mol. Biol. 695 (2011) 17-39.
[7] A. Sionkowska: Biopolymeric nanocomposites for potential biomedical applications. Polymer International 65(10) (2016) 1123-1131.
[8] D.M. Mehta, P.K. Shelat, P.B. Parejiya, A.J. Patel, B. Barot: Investigations of Plantago ovata husk powder as a disintegrating agent for development of famotidine tablets. Int J Pharm Sci Nanotechnol 4(2) (2011) 1412-1417.
[9] M.A. Hussain, G. Muhammad, I. Jantan, S.N.A. Bukhari: Psyllium Arabinoxylan: A Versatile Biomaterial for Potential Medicinal and Pharmaceutical Applications. Polymer Reviews 56(1) (2016) 1-30.
[10] A.O. Elzoghby: Gelatin-based nanoparticles as drug and gene delivery systems: Reviewing three decades of research. Journal of Controlled Release 172 (3) (2013) 1075-1091.
[11] N. Davidenko et al.: Evaluation of cell binding to collagen and gelatin: a study of the effect of 2D and 3D architecture and surface chemistry. J Mater Sci Mater Med 27(10) 2016.
[12] S. Gorgieva, T. Vuherer, V. Kokol: Autofluorescence-aided assessment of integration and μ-structuring in chitosan/gelatin bilayer membranes with rapidly mineralized interface in relevance to guided tissue regeneration. Materials Science and Engineering: C 93 (2018) 226-241.
[13] S. Gorgieva, J. Štrancar, V. Kokol: Evaluation of surface/interface-related physicochemical and microstructural properties of gelatin 3D scaffolds, and their influence on fibroblast growth and morphology. Journal of Biomedical Materials Research Part A 102(11) (2014) 3986-3997.
[14] S. Gorgieva, L. Girandon, V. Kokol: Mineralization potential of cellulose-nanofibrils reinforced gelatine scaffolds for promoted calcium deposition by mesenchymal stem cells. Materials Science and Engineering: C 73 (2017) 478-489.
[15] S. Gorgieva, M. Modic, B. Dovgan, M. Kaisersberger-Vincek, V. Kokol: Plasma-Activated Polypropylene Mesh-Gelatin Scaffold Composite as Potential Implant for Bioactive Hernia Treatment. Plasma Processes and Polymers 12(3) (2015) 237-251.
[16] M. Nikkhah, M. Akbari, A. Paul, A. Memic, A. Dolatshahi-Pirouz, A. Khademhosseini: Gelatin-Based Biomaterials For Tissue Engineering And Stem Cell Bioengineering, in Biomaterials from Nature for Advanced Devices and Therapies, Wiley-Blackwell (2016) 37-62.
[17] F. Zhang et al.: Fabrication of gelatin-hyaluronic acid hybrid scaffolds with tunable porous structures for soft tissue engineering. Int. J. Biol. Macromol. 48(3) (2011) 474-481.
[18] S.-N. Park, J.-C. Park, H.O. Kim, M.J. Song, H. Suh: Characterization of porous collagen/hyaluronic acid scaffold modified by 1-ethyl-3-(3-dimethylaminopropyl)carbodiimide cross-linking. Biomaterials 23(4) (2002) 1205-1212.
[19] T.-W. Wang, M. Spector: Development of hyaluronic acid-based scaffolds for brain tissue engineering. Acta Biomaterialia 5(7) (2009) 2371-2384.
[20] J.M. Lee, H.H.L. Edwards, C.A. Pereira, S.I. Samii: Crosslinking of tissue-derived biomaterials in 1-ethyl-3-(3-dimethylaminopropyl)-carbodiimide (EDC). J Mater Sci: Mater Med 7(9) (1996) 531-541.
[21] K. Jarquín-Yáñez et al.: Structural Effect of Different EDC Crosslinker Concentration in Gelatin- Hyaluronic Acid Scaffolds. Journal of Bioengineering & Biomedical Science 6(2) (2016) 1-6.
[22] B. Kaczmarek, A. Sionkowska, J. Kozlowska, A.M. Osyczka: New composite materials prepared by calcium phosphate precipitation in chitosan/collagen/hyaluronic acid sponge cross-linked by EDC/NHS. International Journal of Biological Macromolecules 107 (2018) 247-253.
[23] N. Zhu, X. Che: Biofabrication of Tissue Scaffolds, in Advances in Biomaterials Science and Biomedical Applications, R. Pignatello, Ed. InTech (2013).
[24] W.-Y. Yeong, C.-K. Chua, K.-F. Leong, M. Chandrasekaran, M.-W. Lee: Comparison of drying methods in the fabrication of collagen scaffold via indirect rapid prototyping. J. Biomed. Mater. Res. Part B Appl. Biomater. 82(1) (2007) 260-266.
[25] D.R. Katti, A. Sharma, K.S. Katti: Chapter 10 - Predictive Methodologies for Design of Bone Tissue Engineering Scaffolds, in Materials for Bone Disorders, S. Bose and A. Bandyopadhyay, Eds. Academic Press (2017) 453-492.
[26] S. Poddar et al.: Fabrication and Cytocompatibility Evaluation of Psyllium Husk (Isabgol)/Gelatin Composite Scaffolds, Appl Biochem Biotechnol (2019). https://doi.org/10.1007/s12010-019-02958-7
[27] N. Varshney et al.: Culturing melanocytes and fibroblasts within three-dimensional macroporous PDMS scaffolds: towards skin dressing material, Cytotechnology 71(1) (2019) 287-303.
[28] G. Nireesha, L. Divya, C. Sowmya, N. Venkateshan, M.N. Babu, V. Lavakumar: Lyophilization/Freeze Drying - An Review. International Journal of Novel Trends in Pharmaceutical Sciences 3(4) (2013).
[29] Basic Cycle Development Techniques For Lyophilized Products [Online]. Available: https://www.pharmaceuticalonline.com/doc/basic-cycle-development-techniques-for-0002.
[30] R.F. Pereira, P.J. Bártolo: Degradation Behavior of Biopolymer-based Membranes for Skin Tissue Regeneration. Procedia Engineering 59 (2013) 285-291.

PREPARATION OF COMPOSITE FILAMENTS AND 3D PRINTS BASED ON PLA MODIFIED WITH CARBON MATERIALS WITH THE POTENTIAL APPLICATIONS IN TISSUE ENGINEERING

Martyna Hunger[1], Wiktor Podgórny[2], Aneta Frączek-Szczypta[1]*

AGH University of Science and Technology,
Al. Mickiewicza 30, 30-059 Krakow, Poland
[1] Faculty of Materials Science and Ceramics,
Department of Biomaterials and Composites,
[2] Faculty of Electrical Engineering Automatics,
Computer Science and Biomedical Engineering,
*e-mail: afraczek@agh.edu.pl

Abstract

This paper discusses the possibilities of obtaining polylactide-based composites and nanocomposites modified with carbon materials using the extrusion method, as well as the potential of their application in 3D printing technology. The aim of this research is to determine the impact of the presence of carbon additives on the properties of composites: mechanical, thermal and chemical. For this purpose, several research techniques were used such as scanning electron microscopy (SEM), X-ray photoelectron spectroscopy (XPS), DSC/TG analysis, infrared Fourier-transform infrared spectroscopy (FTIR) and mechanical tests. It has been shown that it is possible to effectively produce composite materials based on PLA and carbon modifiers after optimization of the extrusion and printing process. Special attention should be paid to the quality of carbon phases homogenization in PLA matrix because the inappropriate dispersion may have a negative effect on the final properties of the composite, especially those modified with nanomaterials. Moreover, the reinforcing effect of carbon phases can be observed, and the quality of obtained filament with carbon fiber after recycling does not differ significantly from the quality of commercially available filaments. The obtained filament was successfully used to print three-dimensional scaffolds. Therefore, both the use of materials which are biodegradable and biocompatible with human tissue and the 3D printing method have the potential to be applied in tissue engineering.

Keywords: *3D printing, poly(lactic acid), carbon materials, scaffold, tissue engineering*

[Engineering of Biomaterials 147 (2018) 7-15]

Introduction

In recent years, composite and nanocomposite materials have been very common due to the unique properties and a very wide range of applications - from technology, industry [1] to medicine and tissue engineering [2-4]. In the latter, biodegradable polymers such as polylactide (PLA) [5-10] or polycaprolactone (PCL) [11-15] deserve special attention. PLA is a thermoplastic polymer that can be obtained from renewable sources [16]. It is popular in biomedical applications due to its relatively good mechanical properties, biocompatibility and biodegradability, as well as simple processing and modification [17,18].

The disadvantage of polymers as biomaterials is frequently too rapid degradation in the physiological environment [19], insufficient mechanical strength and considerable deformability. However, the possibility of introducing modifications makes these materials predominant among the other typically used, e.g. metals [20]. Carbon materials like carbon fibers [21,22] and carbon nanomaterials, such as graphene [23], graphene oxide [12] or carbon nanotubes [24,25] are widely used as additives in polymer composites. Carbon materials are biocompatible with human tissues. They have antibacterial properties, high mechanical strength, and relatively low density. Those properties make the materials very beneficial modifying agents for tissue engineering [26].

There are many traditional methods of composite and nanocomposite biomaterials producing and molding [27]. However, the 3D printing technology, especially Fused Deposition Modeling (FDM) is relatively new and innovative [28]. It is a method of additive manufacturing, waste-free and rapid prototyping, which in general consists in applying subsequent layers of thermoplastic material to the substrate, based on the digital model. A filament with a certain diameter produced by extrusion is used as a semi-finished product. The advantage of additive production in comparison to the standard methods is controllable porosity, individualization of printed objects (patient-specific designs) and a favorable time-cost relation of manufacturing [29,30].

The aim of this research was to determine the effectiveness of extrusion in preparation of composite filaments and assessment of 3D printing (FDM) capabilities in manufacturing composite scaffolds based on carbon fibers and carbon nanomaterials for tissue engineering.

Materials and Methods

Materials

Poly(lactic acid) filament (Barrus Filaments, Holland, d = 1.75 ± 0.05 mm; PLA) was used in this study. The PLA properties are shown in TABLE 1. A commercial filament of poly(lactic acid) with short carbon fiber (Carbon Fiber PLA, Proto-Pasta, USA, 15% w/w SCF, d = 1.75 +/- 0.05 mm; PLA/SCF_C) was used as a reference material. To produce a composite filament, short carbon fibers (SCF_R) were used from the polyacrylonitrile precursor after thermal recycling (SGL Carbon Group, Poland, l = 6 and 12 mm), which were then milled and pressed (FIG. 1). In order to improve homogenization of the carbon fibers with polymer and obtain composite filaments, grinding and pressing of carbon fibers were performed in the PULVERISETTE 16 (Fritsch®) cross-beating mill and on a hand press at 20 MPa, respectively. Graphene oxide (GO) and multi-wall carbon nanotubes functionalized with hydroxyl groups (MWCNT-OH) were obtained from Nanostructured & Amorphous Materials, Inc. (USA). Selected data characterizing carbon nanomodifiers are presented in TABLES 2 and 3.

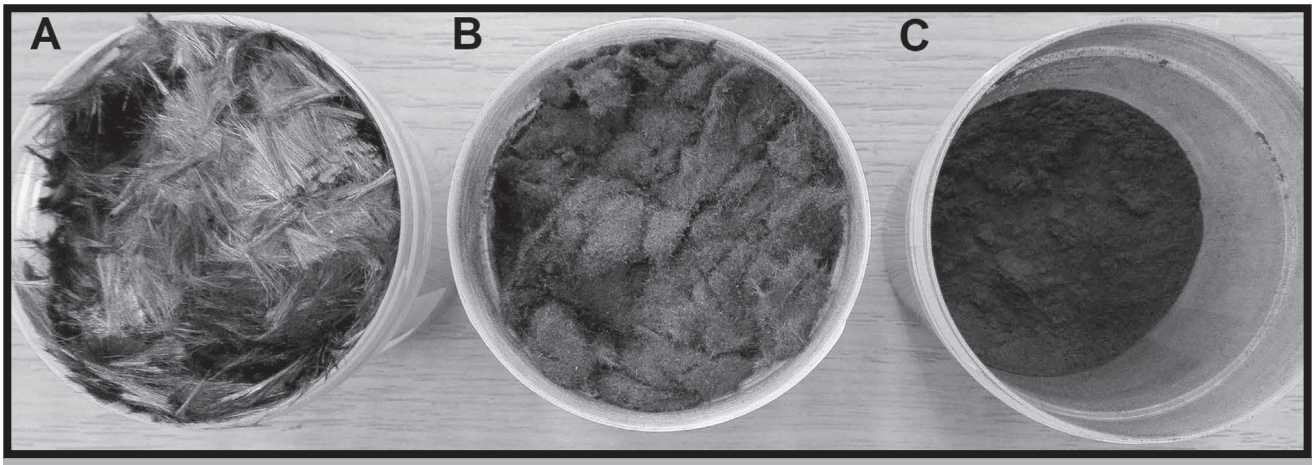

FIG. 1. Carbon fibers after recycling: A) before grinding, B) milled, C) pressed.

TABLE 1. PLA filament properties [31].

Dimensions	
Diameter	**Roundness**
1.75 ± 0.05 mm	≥ 95%
Physical properties	
Specific weight	1.24 g/cm^3
Thermal properties	
Printing temperature	180-210°C
Melting point	145-160°C
Vicat softening temperature	± 60°C

TABLE 2. GO characterization [32].

Purity	> 99 wt%
Diameter	0.5-3 μm
Thickness	0.55-1.2 nm
The number of layers	1-10
Density (at 20°C)	2.1 g/cm^3

TABLE 3. MWCNTs-OH characterization [32].

Purity	> 95 wt%	
Outer diameter	10-20 μm	
Inner diameter	5-10 nm	
Length	0.5-2 μm	
SSA	> 200 m^2/g	
Density (at 20°C)	2.1 g/cm^3	
Content of functional groups [%]	Multi-walled carbon nanotubes (without –OH)	> 95
	-OH	2.91-3.21

TABLE 4. Parameters of the extrusion process.

Nozzle	Custom in-line nozzle, tapering
Extrusion temperature	180°C
Extrusion speed	40 m/h
Diameter of the nozzle	1.75 mm

Methods

Extrusion – filament manufacturing

The extrusion process was carried out using a Filabot extruder (MakerBot®, USA). TABLE 4 presents the parameters of the extrusion process. The commercial PLA filament was cut into small pieces and 50 g of this polymer was introduced into 3 containers to obtain composite PLA filaments with the following additions: SCF_R (15% w/w of PLA; PLA/SCF_R), GO (1% w/w of PLA; PLA/GO) and MWCNT-OH (1% w/w of PLA; PLA/CNT). All the samples were mechanically mixed for 10 min. Each of the obtained mixtures was introduced into the extruder chamber, from where the material in the molten form was transported to the nozzle outlet, and then extruded as a bundle of the filament with a diameter of 1.75 mm. The material was formed in a gravitational manner (the beam freely dropped from a height of 40 cm to a flat surface, self-curling), while the formed material was air-cooled. In each case, the triple extrusion was performed (by re-cutting the obtained filament) to homogenize the materials more efficiently. In addition, pure PLA was also extruded in the same way in order to investigate the influence of extrusion process conditions on the structure and properties of the pure polymer.

3D printing

MakerBot Replicator 2X printer (MakerBot®, USA), based on FDM method was used to the 3D printing of scaffolds. The samples for testing were of a dog-bone shape (FIG. 2) with a 20% hexagonal filling. The purpose of creating such a shape of samples was to assess the possibilities of 3D printing of composite and nanocomposite filaments as well as to evaluate the mechanical properties of the obtained prints. Parameters of the printing process are shown in TABLE 5.

For the selected filaments, test prints of 3D scaffolds were also made. In order to create a correct scaffold model consistent with the assumptions, Autodesk Inventor® Professional 2017 was used. It is software with professional tools that enable 3D design of mechanical elements, their documentation and simulation of products. For the needs of the work, basic functions of the software were used, i.e. tools for parametric 3D design. Designs of the scaffolds serving as the basis for the prints are shown in FIG. 3.

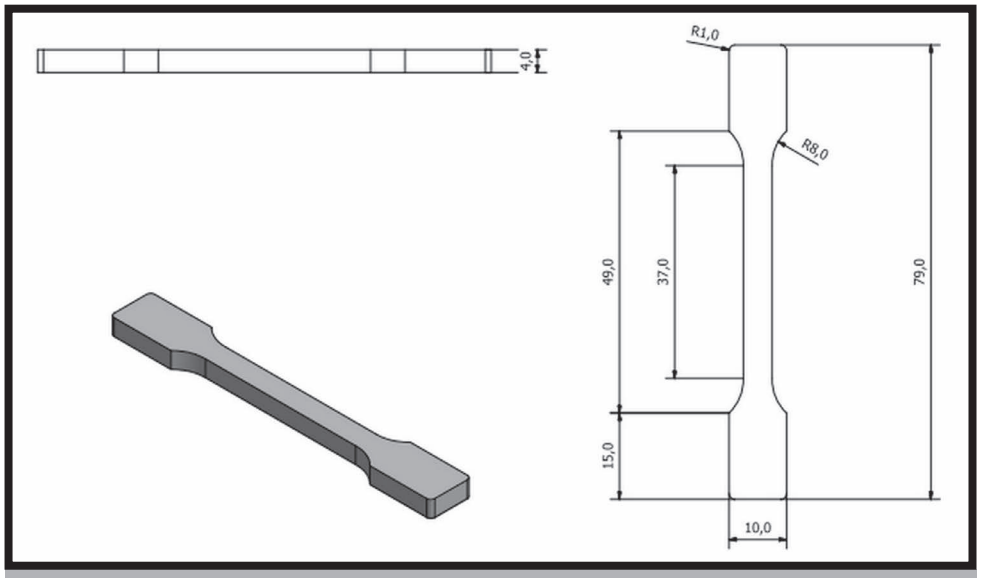

FIG. 2. Sample design (dog-bone) used for 3D printing.

TABLE 5. Parameters of 3D printing process.

Extruder temperature	200°C (PLA) 220°C (composites)
Platform temperature	30°C
Nozzle diameter	0.3 mm
Printing speed	50 mm/s (PLA) 35 mm/s (composites)
Layer height	0.2 mm
Number of shells	2
Thickness of external layers (top and bottom)	0.6 mm
Parameters of the sample (dogbone shape)	
Sample dimensions	79x10/5x4 mm
Infill	hexagonal
Infill density	20%

Characterization of carbon materials

The microstructure characterization of carbon additives was performed using SEM images (NOVA NanoSEM 200 (FEI™)) were made to measure fiber diameters and lengths after recycling and to compare them to commercial filament fibers, as well as to determine the fiber reinforcement effect. To check PLA matrix reinforcement effect, critical lengths of the fibers for both SCF_R and SCF_C were calculated. For this purpose, the formula 1 was used [49]:

$$l_{cr} = \frac{R_m d_m}{2\tau_o} \quad (1)$$

R_m – matrix strength [MPa]
(value given by the producer $R_m \approx 130$ MPa),
d_m – fiber diameter [μm],
τ_o – shear strength of the matrix (for PLA ~ 20 MPa)

Determination of the critical fiber length, above which the material strengthens, allowed determining which carbon fibers fulfil the criterion:

$$l_{cr} < l < 10\, l_{cr} \quad (2)$$

l_{cr} – critical fiber length, l – fiber length

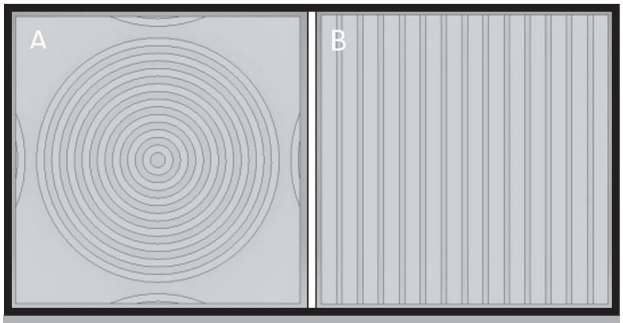

FIG. 3. Scaffolds designed in the Autodesk Inventor® Professional 2017 program: A) ring, B) linear.

XPS (Scanning XPS Microprobe PHI 5000 VersaProbell) was used to perform quantitative analysis of the chemical composition and to determine the types of chemical bonds occurring between elements on the surface of the tested carbon materials. The source of X-ray radiation was monochromatic Al Kα. The diameter of the beam was 100 μm, and the analysis surface φ 100 μm (25 W (4 mA, 15 kV)) at the charge neutralization Ar^+ -8 eV, e^- -1 eV. The analyzer resolution for the reference and detailed spectra was 117 eV and 46,95 eV, respectively.

Characterization of filaments

Having obtained the filaments, their diameters were measured and a macroscopic evaluation was made. Microscopic observations using SEM (NOVA NanoSEM 200 (FEI™)) were also performed to analyze the distribution of carbon phases in the polymer matrix.

Additionally, a static tensile test was carried out (Zwick 1435, Germany). Properties such as tensile strength, Young's modulus, relative strain and rupture work were evaluated. Parallel specimen length and the test speed were 40 mm and 50 mm/min, respectively. The Young's modulus determination was measured in the range of 30-50 N.

FTIR (Bruker Tensor 27 FTIR-ATR) was used to check and determine possible structural changes of the polymer as a result of several thermal treatments (thermal degradation) as well as changes caused by the presence of carbon additives (in particular nanomaterials). The wavelength range was between 4000 and 500 cm^{-1}, and the number of scans was 64. The test in the absorption mode was carried out using a diamond crystal, by Attenuated Total Reflectance (ATR).

DSC/TG measurements were made with the NETZSCH STA 449 F3 Jupiter®. The temperature of the test ranged from 40 to 600°C, while the heating rate was 10 K/min. In the DSC part graphs of the heat flow versus temperature were recorded, while in the TG part - the relation between the percentage loss of mass and temperature.

Characterization of the samples after printing

The printed samples shaped as dog-bones were evaluated macroscopically and compared in various aspects. To assess the practical obtaining possibilities of the samples, they were examined for mechanical properties. The static tensile test was performed in the same way as it was conducted on filaments (section 2.2.4).

Characterization of three-dimensional scaffolds

Measurements and macroscopic observations were also run on printed scaffolds. The comparative evaluation of the actual prints and the digital models was performed via microscopic observation and dimensional analysis (Keyence VHX-900F digital microscope). The tested parameter was the height of the scaffolds, measured on the basis of 3D images using tools that allow microscopic measurements attached as microscope software.

Results and Discussion

On the basis of SEM measurements (FIG. 4) it can be concluded that the manual pressing caused changes in the length of the fibers. On average, SCF_C lengths are almost twice as short as the SCF_R ones. In both cases, a significant length distribution is seen, although the SCF_R are more homogeneous. Determination of critical lengths based on the formula 1 led to the conclusion that carbon fibers obtained from both the commercial filament and the recycled filament meet the criterion (formula 2) providing the proper material reinforcement.

XPS measurement results (TABLE 6) determined the chemical composition on the surface of SCF_C, SCF_R, MWCNTs-OH and GO. Analysis of chemical states of C1s in carbon fibers showed their higher content in SCF_R. SCF_C were obtained for testing by dissolving the polymer matrix and could have a polymer on their surface.

TABLE 6. Atomic concentration of elements measured on the surface of the carbon materials.

Sample	C [%]	O [%]	N [%]
SCF_C	76.11	22.61	1.06
SCF_R	88.47	7.90	3.61
MWCNTs-OH	97.20	2.76	0.00
GO	66.83	31.26	1.30

Images of the obtained filaments are shown in FIG. 5. The similarity of PLA/SCF_R to PLA/SCF_C is noticeable. The average of the filament diameter value PLA/SCF_R was the closest to the diameter of the commercial filament (TABLE 7). Relatively low standard deviation shows a high homogeneity of the diameter along the entire length of the filament. The worst geometric parameters show PLA/GO. Its diameter had the lowest value, and the standard deviation was relatively high, which indicates a heterogeneity along the length of the filament. This is most likely due to the lack of sufficient homogenization of the GO in the sample. Graphene oxide tends to agglomeration and is less wetted by the polymer than other additives.

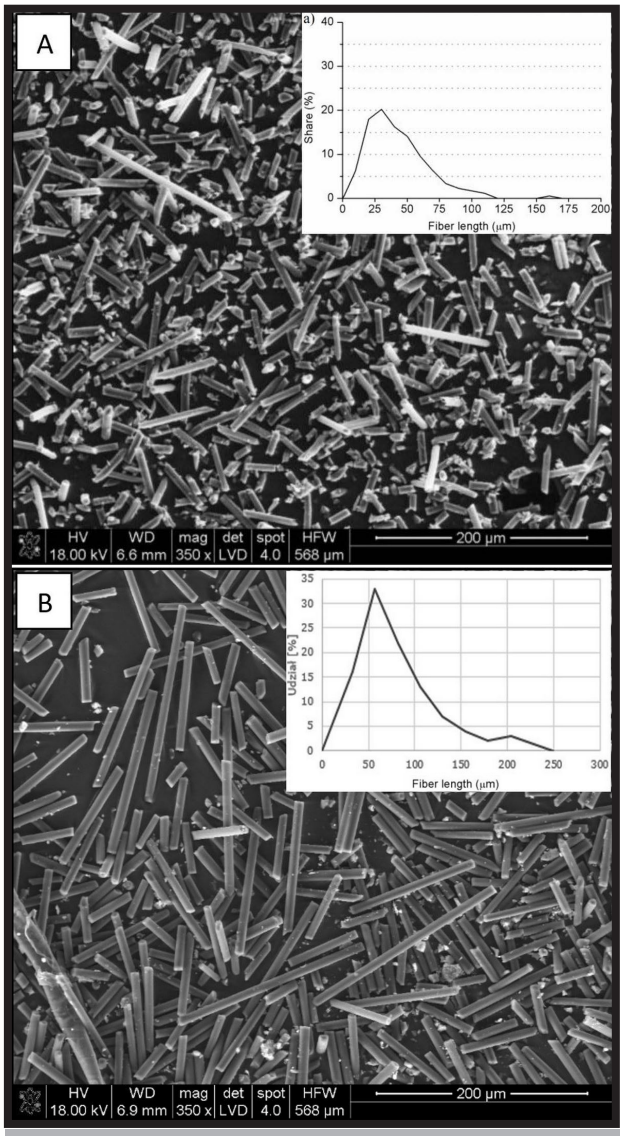

FIG. 4. SEM images (mag. 350x) and histograms: A) SCF_R, B) SCF_C.

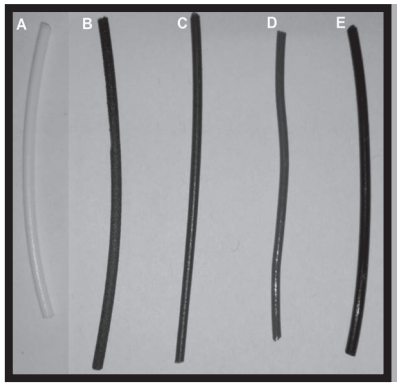

FIG. 5. Images of fragments of the obtained filaments: A) PLA, B) PLA/SCF_C, C) PLA/SCF_R, D) PLA/GO, E) PLA/CNT.

TABLE 7. Values of diameters of the obtained and the commercial filaments.

Filament	Diameter ± SD [mm]
PLA	1.75 ± 0.05
PLA/SCF_C	1.75 ± 0.05
PLA/SCF_R	1.57 ± 0.06
PLA/GO	1.41 ± 0.12
PLA/CNT	1.54 ± 0.09

SEM images of filaments cross-sections are shown in FIG 6. The images show that PLA/SCF_C has the best distribution of the reinforcing phase, and the homogenization of fibers for PLA/SCF_R is similar. Much worse distribution of the reinforcing phase is observed in the polymer nanocomposites. On the PLA/GO and PLA/CNT cross-sections (FIG. 6b and 6d), both the areas with larger agglomerates of the nanomaterial (black circles), as well as areas without modifying phase in form of agglomerates (white circles) are visible.

The results of mechanical tests are presented in TABLE 8. Among the obtained composites filaments, PLA/CNT has the highest tensile strength and this value is the same as for PLA/SCF_C. In turn, the nanotubes due to their characteristic structure transfer stresses better than graphene oxide. PLA/GO shows the lowest tensile strength and Young's modulus, which probably results from poor GO homogenization in the polymer matrix. On the basis of the obtained results, it can also be concluded that the production of filament PLA/SCF_R by extrusion is effective. Its tensile strength does not differ significantly from the commercial PLA/SCF_C filament. Only Young's modulus is about 30% lower in comparison with commercial filament (PLA/SCF_C). For this reason, a filament with recycled carbon fibers can be used to obtain materials that do not require the transfer of large forces. One such application can be scaffolds for tissue regeneration, taking into account the biocompatibility of carbon fibers.

TABLE 8. Results after tensile test of filaments.

	R_m ± SD [MPa]	Young's Modulus ±SD [GPa]	Strain ε ± SD [%]	Rupture work ± SD [N·mm]
PLA	59.88 ± 5.26	2.92 ± 0.17	2.80 ± 0.43	79.96 ± 20.16
PLA/SCF_C	62.63 ± 6.59	5.15 ± 0.64	1.71 ± 0.22	59.52 ± 13.61
PLA/SCF_R	60.30 ± 6.82	3.60 ± 0.81	2.58 ± 0.75	75.97 ± 29.25
PLA/GO	52.58 ± 5.98	2.04 ± 0.30	4.24 ± 0.92	90.01 ± 35.45
PLA/CNT	62.00 ± 4.65	2.68 ± 0.27	3.14 ± 0.11	77.12 ± 9.26

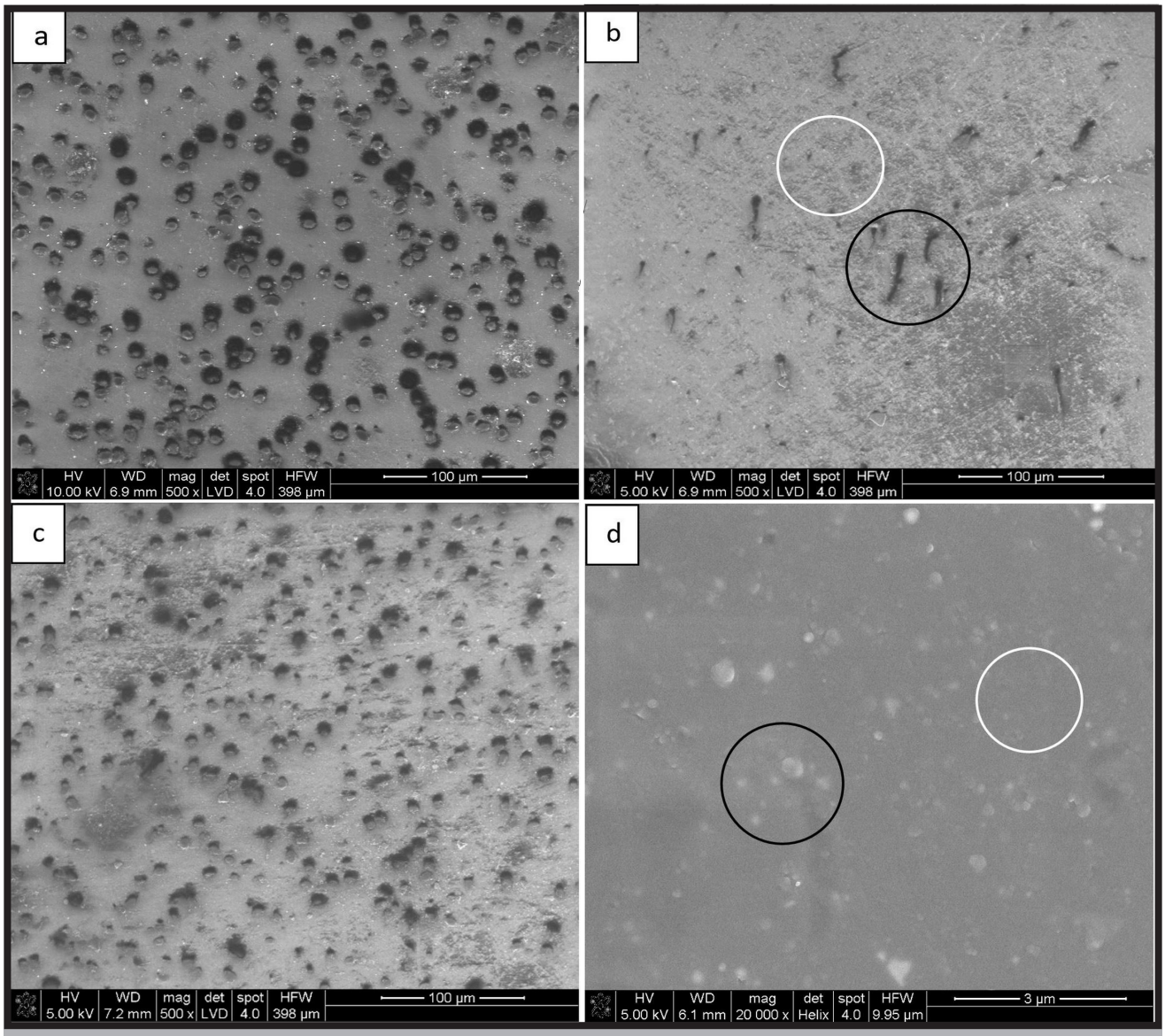

FIG. 6. SEM images of the filament cross-sections: a) PLA/SCF_C (mag. 500x), b) PLA/GO (mag. 500x), c) PLA/SCF_R (mag. 500x), d) PLA/CNT (mag. 20000x).

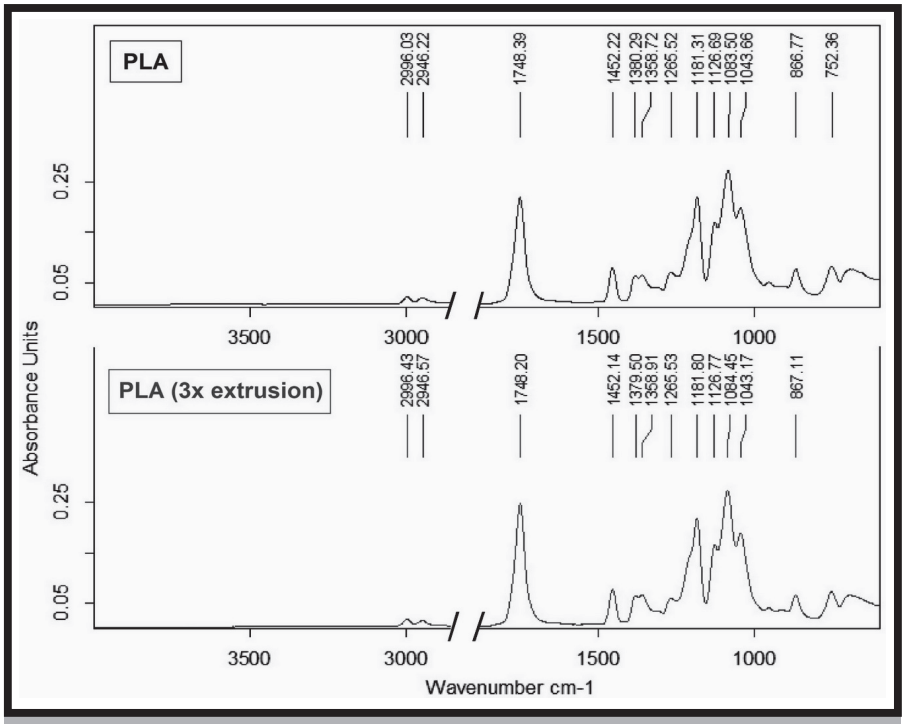

FIG. 7. FTIR spectrum for PLA and PLA after triple extrusion.

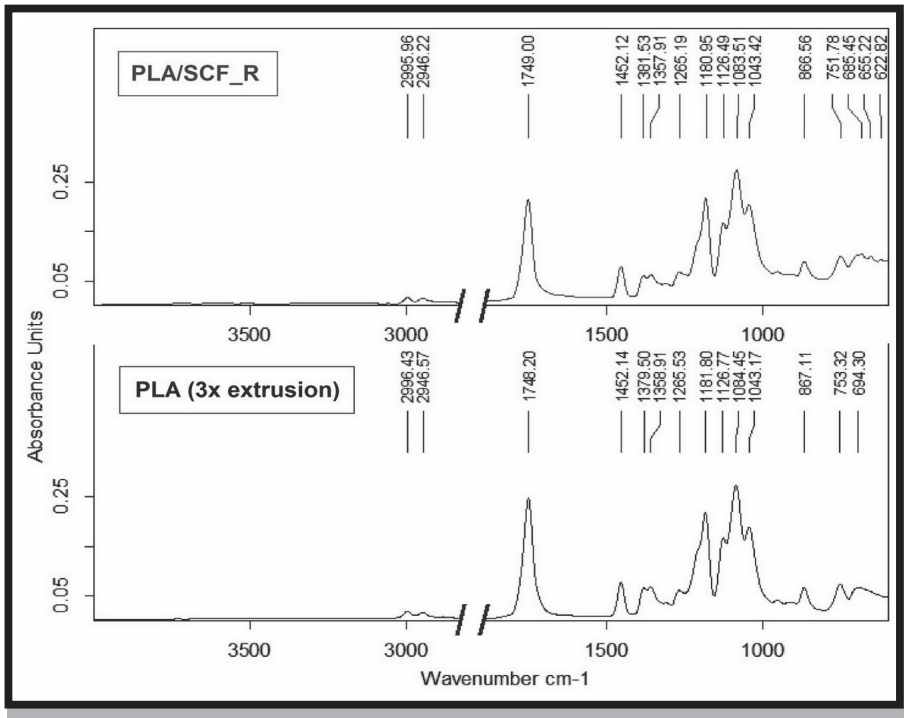

FIG. 8. FTIR spectrum for PLA/SCF_R and PLA after triple extrusion.

FTIR-ATR spectroscopic measurements did not show the effect of both the temperature during the triple extrusion and the presence of carbon additives on structural changes of PLA. Comparative spectra for PLA with PLA after triple extrusion and PLA after triple extrusion with PLA/SCF_R are shown in FIGs 7 and 8, respectively. They do not show significant changes in spectra - characteristic bands occur at the same wavelengths. The characteristic band at the 1748 cm^{-1} is derived from the stretching vibrations of C=O. In turn, the bands at the wavenumbers 1181 and 1083 cm^{-1} are the result of the stretching vibrations coming from the single C-O bond. The subtle bands at 1452 cm^{-1}, 1380 cm^{-1}, and 1358 cm^{-1} are derived from the bond of C-H.

DSC/TG tests showed an insignificant impact of the triple extrusion and the presence of carbon additives on the characteristic temperatures of PLA (FIG. 9 and 10). The DSC results for the PLA and PLA after triple extrusion show that the thermal processing of the polymer has an impact on reducing the degradation temperature about 20°C. From the TG plot for filaments with carbon fiber PLA/SCF_C and PLA/SCF_R, it appears that residues at 600°C were 15.20 and 13.14%, respectively (FIG. 11). Taking into account the assumed concentration of carbon phases (15% w/w), it can be concluded that the remnants after the thermal test were carbon fibers. However, a lower value for recycled fibers (PLA/SCF_R) may result from a lower real weight concentration of the modifier in the polymer. During the filament manufacturing, some of the fibers could have been deposited in the extruder chamber, thereby not mixing with the polymer.

Photographs of printed dogbone shape samples are presented in FIG. 12. The quality of the printed samples shows that the obtained filaments can be used in a 3D printer. The sample with the best quality is PLA/SCF_R (FIG. 12C) - it can be seen that it does not significantly differ from the commercial sample (FIG. 12B). 3D printing of this material was carried out without major complications (FIG. 13).

The results of the tensile test of the dogbone shape samples are shown in TABLE 9. The highest tensile strength was observed for PLA/CNT. Relative strain and destructive work are also the highest in this case. Slightly worse of these parameters, although the higher Young's modulus was observed for PLA/SCF_R sample. For the nanocomposite PLA/GO, relatively low mechanical parameters were noted, which was also found in the study of PLA/GO filament. This is another confirmation of the lack of sufficient homogenization of the GO in polymers matrix. High relative strain value indicates that tensile stresses were mainly transmitted through the polymer matrix.

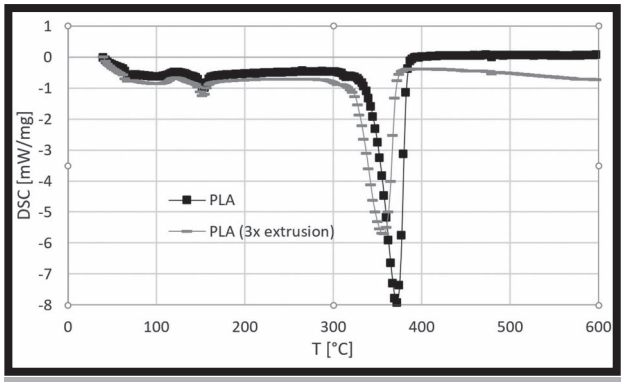

FIG. 9. DSC curve for PLA and PLA after triple extrusion.

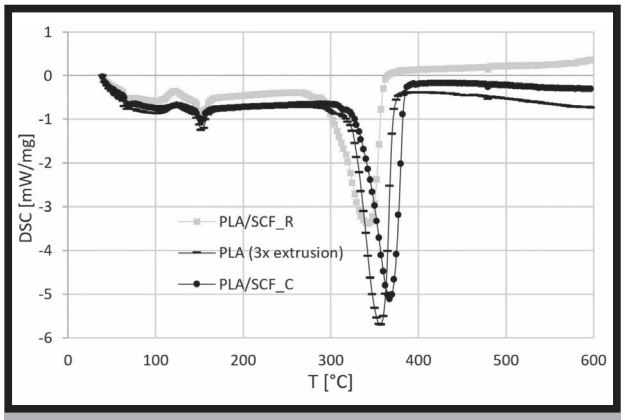

FIG. 10. DSC curves for PLA after triple extrusion and for composite filaments: PLA/SCF_R, PLA/SCF_C.

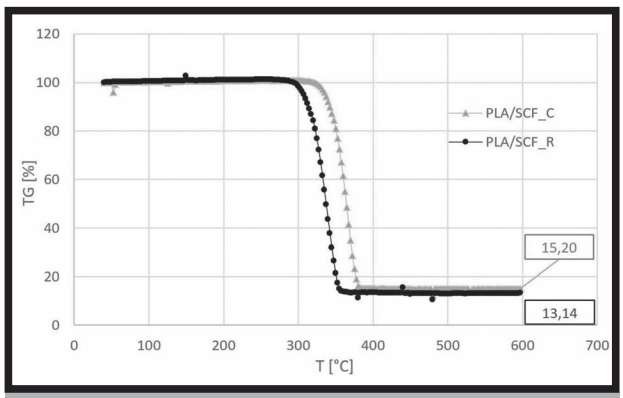

FIG. 11. TG curve for PLA/SCF_R, PLA/SCF_C samples.

FIG. 12. 3D printed dogbone shape samples: A) PLA, B) PLA/SCF_C, C) PLA/SCF_R, D) PLA/GO, E) PLA/CNT.

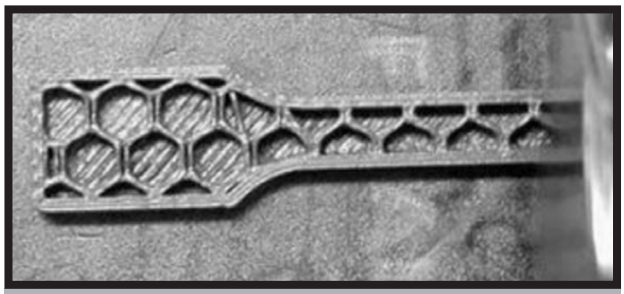

FIG. 13. Hexagonal infill (20%) of the PLA/SCF_R sample.

TABLE 9. Results of tensile test of the 3D printed samples.

	R_m ± SD [MPa]	Modulus ± SD [GPa]	Strain ε ± SD [%]	Rupture work ± SD [N·mm]
PLA	36.30 ± 3.63	1.23 ± 0.12	3.93 ± 0.39	698.94 ± 69.90
PLA/SCF_C	39.00 ± 0.57	2.10 ± 0.06	3.17 ± 0.15	648.61 ± 24.66
PLA/SCF_R	38.47 ± 6.21	2.02 ± 0.26	3.04 ± 0.21	633.75 ± 158.96
PLA/GO	31.68 ± 2.33	1.23 ± 0.07	3.62 ± 0.31	604.74 ± 101.19
PLA/CNT	38.98 ± 2.07	1.32 ± 0.08	4.07 ± 0.13	814.54 ± 80.01

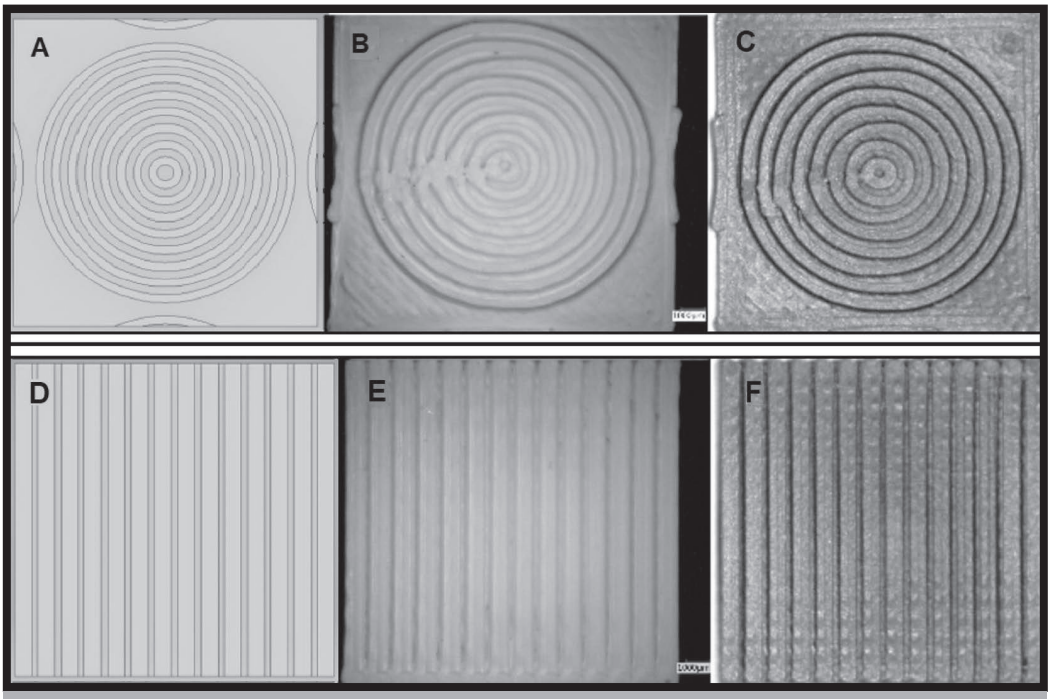

FIG. 14. Digital models and printed scaffolds: A) ring model, B) PLA ring scaffold, C) PLA/SCF_R ring scaffold, D) linear model, E) PLA linear scaffold, F) PLA/SCF_R linear scaffold.

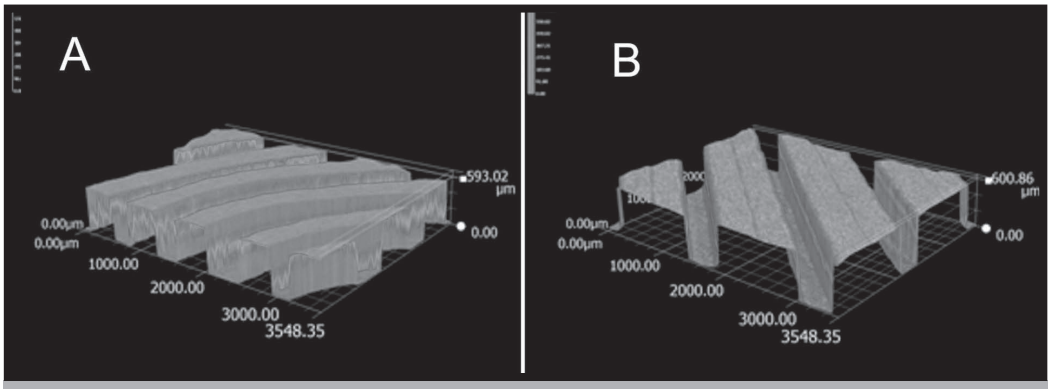

FIG. 15. 3D images of microstructure of printed scaffolds: A) ring, B) linear.

3D printing of scaffolds

After optimizing the printing process, 3D prints of the pure PLA scaffolds and composites scaffolds obtained from PLA/SCF_R filament were made. The choice of this composite material for printing of the scaffolds resulted from the analysis of results for all filaments and dogbone shape samples. Filament PLA/SCF_R was characterized by the highest quality as well as optimal mechanical parameters. Also, the PLA/SCF_R dogbone shape samples showed the most favorable properties. FIG. 14 presents photographs of 3D scaffolds printed from PLA and PLA/SCF_R filaments with images of digital models of individual designs. The obtained scaffolds retain their designed shape, however, greater dimensional stability is shown by the linear structure than the ring structure. The dimensional analysis made on digital microscope allowed to obtain 3D images of printed scaffolds (FIG. 15). The calculations based on digital visualization show that the real height of the PLA/SCF_R ring and linear structures is smaller than the assumed by 30% and 17%, respectively (FIG. 16). The lower value of the height of the printed paths in scaffolds results most probably from the spreading of the melted polymer bundle of due to the action of gravity. This effect should be taken into account when designing further scaffolds.

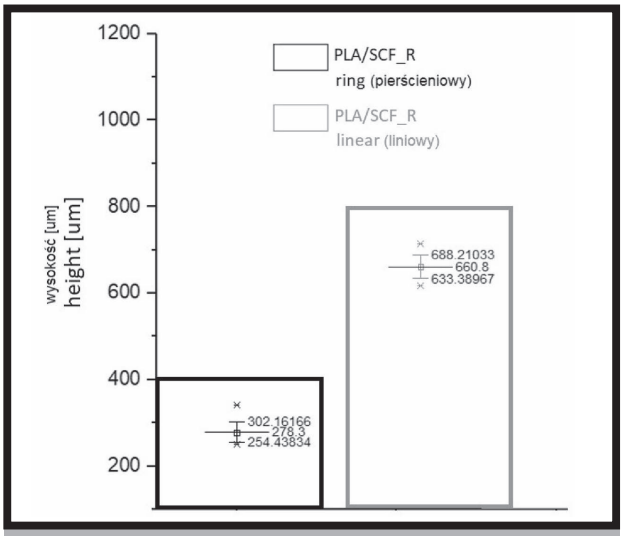

FIG. 16. Results of the analysis of topography changes in PLA/SCF_R scaffolds - average values, standard deviations and outliers; bar charts show the expected values in accordance with the project.

Conclusions

This paper presents the 3D printing process using the FDM method, starting from the selection of materials, through the complicated filament production procedure, to its use in a 3D printer, as well as optimizing the printing process and obtaining the desired objects. Based on the conducted experiments, it can be concluded that the whole process is quite complex, requires knowledge and experience demanding experience without which it is practically impossible to obtain high-quality materials. Despite numerous difficulties during filament production and 3D printing, composite printing is possible, and if the filament formation process will be optimized and the materials will be properly homogenized, the entire technology of self-generation of composite and nanocomposite objects with a polymer matrix using the 3D printing method can be fast and very effective. In addition, it is highly desirable to use recycled materials, so the method has both economic and ecological benefits. Moreover, the possibility of using biodegradable and biocompatible with the human body materials makes this technology has potential and can be an alternative in producing prototypes and forming scaffolds for tissue engineering.

Acknowledgments

The study was financed from the statute funds of AGH-UST, Faculty of Materials Science and Ceramics, Project no. 11.11.160.182.

References

[1] E. Bayraktar: Reference Module in Materials Science and Materials Engineering. Composites Materials, Elsevier (2017)
[2] M. Ramalingam, S. Ramakrishna: Nanofiber Composites for Biomedical Applications. Elsevier (2017)
[3] G. Turnbull et al.: 3D bioactive composite scaffolds for bone tissue engineering. Bioactive Materials 3(3) (2018) 278-314.
[4] M.S. Scholz et al.: The use of composite materials in modern orthopaedic medicine and prosthetic devices: A review. Composite Science and Technology 71(16) (2011) 1791-1803.
[5] I. Armentano et al.: Multifunctional nanostructured PLA materials for packaging and tissue engineering. Progress in Polymer Science 38, (10-11) (2013) 1720-1747.
[6] I.J. Macha et al.: In vitro study and characterization of cotton fabric PLA composite as a slow antibiotic delivery device for biomedical applications. Journal of Drug Delivery Science and Technology 43 (2018) 172-177.
[7] Y. Liu et al.: Composite poly(lactic acid)/chitosan nanofibrous scaffolds for cardiac tissue engineering. International Journal of Biological Macromolecules 103 (2017) 1130-1137.
[8] C. Zhao et al.: Development of PLA/Mg composite for orthopedic implant: Tunable degradation and enhanced mineralization. Composites Science and Technology 147 (2017) 8-15.
[9] S. Tajbakhsh, F. Hajiali: A comprehensive study on the fabrication and properties of biocomposites of poly(lactic acid)/ceramics for bone tissue engineering. Materials Science and Engineering: C 70, Part 1, (2017) 897-912.
[10] C. Yang et al.: A facile electrospinning method to fabricate polylactide/graphene/MWCNTs nanofiber membrane for tissues scaffold. Applied Surface Science 362 (2016) 163-168.
[11] S. Jatteau et al.: A tubular polycaprolactone/hyaluronic acid scaffolds for nasal cartilage tissue engineering. Engineering of Biomaterials 141 (2017) 8-12.
[12] S. Yildirim et al.: Preparation of polycaprolactone/graphene oxide scaffolds: A green route combining supercritical CO_2 technology and porogen leaching. The Journal of Supercritical Fluids 133, Part 1 (2018) 156-162.
[13] E. Murray et al.: Enzymatic degradation of graphene/polycaprolactone materials for tissue engineering. Polymer Degradation and Stability 111 (2015) 71-77.
[14] E. Torres et al.: Improvement of mechanical and biological properties of Polycaprolactone loaded with Hydroxyapatite and Halloysite nanotubes. Materials Science and Engineering: C 75 (2017) 418-424.
[15] S. Mallakpour, N. Nouruzi: Polycaprolactone/metal oxide nanocomposites: An overview of recent progress and applications, Biodegradable and Biocompatible Polymer Composites (2018) 223-263.
[16] J.R. Dorgan et al.: Polylactides: properties and prospects of an environmentally benign plastic from renewable resources. Macromolecular Symposia 175(1) (2001) 55-66.
[17] E. Castro-Aguirre et al.: Poly(lactic acid)-Mass production, processing, industrial applications, and end of life. Advanced Drug Delivery Reviews 107 (2016) 333-366.
[18] D. da Silva et al.: Biocompatibility, biodegradation and excretion of polylactic acid (PLA) in medical implants and theranostic systems. Chemical Engineering Journal 340 (2018) 9-14.
[19] F.P. La Mantia et al.: Degradation of polymer blends: A brief review, Polymer Degradation and Stability 145 (2017) 79-92.
[20] N.S. Yatigala et al.: Compatibilization improves physico--mechanical properties of biodegradable biobased polymer composites. Composites Part A: Applied Science and Manufacturing 107 (2018) 315-325.
[21] P. Huang et al.: 3D printing of carbon fiber-filled conductive silicon rubber. Materials & Design 142 (2018) 11-21.
[22] R.T.L. Ferreira et al.: Experimental characterization and micrography of 3D printed PLA and PLA reinforced with short carbon fibers. Composites Part B: Engineering 124 (2017) 88-100.
[23] E. Murray et al.; Enzymatic degradation of graphene/polycaprolactone materials for tissue engineering. Polymer Degradation and Stability 111 (2015) 71-77.
[24] A. Pantano: Mechanical Properties of CNT/Polymer, Carbon Nanotube-Reinforced Polymers, From Nanoscale to Macroscale, Micro and Nano Technologies (2018) 201-232.
[25] K. Kim et al.: 3D printing of multiaxial force sensors using carbon nanotube (CNT)/thermoplastic polyurethane (TPU) filaments. Sensors and Actuators A: Physical 263 (2017) 493-500.
[26] K. Mitura, P.K. Zarzycki: Biocompatibility and Toxicity of Allotropic Forms of Carbon in Food Packaging, Role of Materials Science in Food Bioengineering. Handbook of Food Bioengineering (2018) 73-107.
[27] N.G. Shimpi: Biodegradable and Biocompatible Polymer Composites - Processing, Properties and Applications. Composite Science and Engineering (2017)
[28] N. Aliheidari et al.: Fracture resistance measurement of fused deposition modeling 3D printed polymers. Polymer Testing 60 (2017) 94-101.
[29] Y. Deng, J. Kuiper: Extrusion-based 3D printing technologies for 3D scaffold engineering, Functional 3D Tissue Engineering Scaffolds - Materials, Technologies and Applications (2017)
[30] M. Guvendiren et al.: Designing Biomaterials for 3D Printing, ACS Biomaterials Science & Engineering 2(10) (2016) 1679-1693.
[31] www.barrus.pl (10.02.2018)
[32] www.nanoamor.com (28.08.2018)

SURFACE FUNCTIONALIZATION OF POLY(L-LACTIDE-*CO*-GLYCOLIDE) MEMBRANES WITH AMPHIPHILIC POLY(2-OXAZOLINE) FOR GUIDED TISSUE REGENERATION AND TREATMENT OF BONE TISSUE DEFECTS

Anna Maria Tryba[1], Małgorzata Krok-Borkowicz[1], Czesława Paluszkiewicz[2], Elżbieta Pamuła[1]*

[1] AGH University of Science and Technology,
Faculty of Materials Science and Ceramics,
Department of Biomaterials and Composites,
Al. Mickiewicza 30, 30-059 Kraków, Poland
[2] Institute of Nuclear Physics,
Polish Academy of Sciences,
ul. Radzikowskiego 152, 31-342 Kraków, Poland
*e-mail: epamula@agh.edu.pl

Abstract

The main challenge of this research was to functionalize the surface of poly(L-lactide-co-glycolide) (PLGA) membranes with amphiphilic poly(2-oxazoline) (POx) in order to change PLGA chemical state and properties. Poly(2-oxazolines) are very powerful polymers, which thanks to active pendant groups can be easily functionalized with biologically active molecules or peptides. The membranes were prepared by dissolving PLGA, POx, and poly(ethylene glycol) (PEG, 1000 Da) in methylene chloride (DCM), followed by PEG leaching. POx molecules were preferentially adsorbed at the interface PLGA-POx-PEG thanks to affinity to both hydrophilic (PEG) and hydrophobic (PLGA) chains. The properties of the membranes were characterized with Fourier transform infrared spectroscopy (FTIR), scanning electron microscopy (SEM) and wettability tests. Cytocompatibility of the materials in contact with osteoblast-like MG-63 cells was studied by evaluation of cell viability (Alamar-Blue test), live/dead and phalloidin/DAPI staining. The results show that the presence of POx influenced topography of the PLGA membranes, but did not have an impact on their wettability. All membranes were found cytocompatible with model osteoblasts. Presence of POx resulted in better cell adhesion as shown by microscopic studies after fluorescence staining for nuclei and cytoskeleton actin filaments. In summary, one-step phase separation process between PLGA, PEG, and POx, dissolved in DCM followed by drying and PEG leaching resulted in cytocompatible PLGA membranes with immobilised POx, which might be considered for guided tissue regeneration technique in periodontology and in bone tissue engineering.

Keywords: *poly(L-lactide-co-glycolide), poly(ethylene glycol), poly(2-oxazolines), phase separation, Fourier transform infrared spectroscopy (FTIR), osteoblast--like cells, guided tissue regeneration (GTR), bone tissue engineering*

[Engineering of Biomaterials 147 (2018) 16-20]

Introduction

Impaired bone healing is a crucial clinical problem in orthopedics, oral and maxillofacial surgery, and periodontology. Medical devices enhancing bone repair and healing should be made of biomaterials with adequate properties, such as biocompatibility, bioactivity, osteoconduction, and biodegradation [1,2]. Particularly interesting form of biomaterials are membranes, which are widely used in artificial organs and diagnostic devices. They can be also used in periodontal applications and act as barriers in guided tissue regeneration (GTR) to protect bony defects from the invasion of connective tissue and mucous membrane, and assure adequate conditions for regeneration of bone tissue [1,3,4].

Poly(L-lactide-co-glycolide) (PLGA) has been often applied to create scaffolds for bone tissue engineering and membranes for periodontology [5]. Several strategies have been used to fabricate PLGA membranes, for example, porogen leaching, fibers bonding or phase separation [3,6]. A key feature of PLGA is its degradation by hydrolysis. The final degradation products of PLGA, i.e. lactic and glycolic acids are removed by natural metabolic pathways [5]. However, despite being biocompatible, clinical application of PLGA for bone regeneration and GTR is hampered by poor osteoconductivity and lack of cell adhesion motifs such as arginine-glycine-aspartic acid (RGD), which are beneficial for cell adhesion controlled by interaction with integrins [7].

Poly(2-oxazolines) (Pox) are amphiphilic, non-ionic polymers, which are synthesised *via* living cationic polymerization [8]. They are biocompatible and have been used in medical and drug delivery applications. They can be conjugated with drugs, peptides and proteins, e.g. RGD [9].

A successful approach in biomaterials science is to design the surface properties of approved materials for specific medical application. The main challenge in this area is the development of processing routes allowing for simple and efficient surface modification of complex shaped geometries. Thus, our research aimed at surface functionalization of PLGA membranes *via* phase separation between PLGA, water-soluble poly(ethylene glycol) (PEG) and amphiphilic bifunctional POx [10]. Physicochemical and biological properties of resulting membranes important from the point of view of periodontology and bone tissue engineering applications were analyzed and described in this paper.

Materials and Methods

Materials

The membranes were made from PLGA (85:15, 100 kDa, d = 1.9, synthesised at Centre of Polymer and Carbon Materials, Polish Academy of Sciences in Zabrze, Poland) [11]. As a solvent DCM and as a pore former PEG (1000 Da), both from Sigma-Aldrich, were used. As an amphiphilic POx molecule poly(2-metyl-2-oxazoline-b-2-butyl-2-oxazoine-b-2-metyl-2-oxazoline) and more specifically methyl-P[$MeOx_{37}$-b-$BuOx_{19}$-b-$MeOx_{29}$-piperidine(P2—P2) (Mn = 8 kDa, d = 1.14, synthesized at Technische Universität Dresden, Germany) [12] was used.

Manufacturing methods

PLGA and PEG were co-dissolved in DCM at a concentration of 10% wt/vol and 1 wt% POx in respect to PLGA was added. The membranes PLGA-POx were obtained by solvent casting on glass Petri dishes, followed by air drying for 24 h and vacuum drying for 24 h. Afterwards, PLGA-POx-PEG blends were washed in purified water for 5 days; water was exchanged every 30 min during day 1 and every 2 h during days from 2 to 5.

As references PLGA membranes and PLGA foils without POx were made by dissolving PLGA in DCM at a concentration of 10%, slip casting on Petri dishes, followed by air drying for 24 h and vacuum drying for 24 h.

Evaluation methods

FTIR in attenuated total reflection mode (ATR) with ZnSe crystal has been used for the characterization of main ingredients used in membranes preparation, i.e. PLGA, PEG and POx, as well as obtained PLGA-PEG-POx blend, PLGA-POx membrane and PLGA foil. FTIR spectra were recorded on Nicolet iS5-iD5 spectrometer with resolution of 4 cm^{-1}.

Water contact angle values were measured on DSA Mk2 (Krüss, Germany) using ultra-high purity water (UHQ-water, Pure-Lab, UK) droplets of 0.20 µl. Droplets were deposited on the surfaces at room temperature, and their images were recorded using a video camera and analyzed using an image analysis system (DSA software). The results were expressed as the average and standard deviation (S.D.) of 10 droplets deposited on the surface of the samples.

Microstructure of the samples was assessed with scanning electron microscopy (SEM, Nova Nano SEM 200, USA, secondary electron mode).

Cytocompatibility tests were performed on osteoblast-like MG-63 cells. Prior to the experiment, the samples were placed in the wells of 24-well plates, incubated in 70% ethanol for 10 min, then the samples were transferred to 48-well plates and left under the laminar hood and UV lamp overnight for sterilization. $8x10^3$ cells suspended 1 ml cell culture medium (EMEM, ATTC, USA) supplemented with 10% fetal bovine serum, 1% penicillin/streptomycin, 0.1% amino acids and sodium pyruvate (PAA, Germany) were poured on the samples and cells were cultured at 37°C under a humidified atmosphere with 5.0% CO_2 for 24 and 72 h. Cell viability was evaluated using AlamarBlue reagent (In Vitro Toxicology Assay Kit, resazurin based, Sigma-Aldrich) and live/dead staining using 1 ml of PBS supplemented with 1 µl (1 mg/ml) of calcein AM (Sigma) and 1 µl (1 mg/ml) of propidium iodide (Sigma). The cells were also stained for phalloidin/DAPI to visualize actin fibers and nuclei, respectively. The samples were washed twice in PBS and observed under a fluorescence microscope (Zeiss Axiovert 40, Carl Zeiss, Germany). Statistical analysis was performed using a one-way analysis of variance (one-way ANOVA). Significant differences were assumed at $*p < 0.05$. The results were presented as mean ± S.D.

Results and Discussion

FIG. 1 shows FTIR-ATR spectra of main ingredients: PLGA, PEG 1000 and POx. In PLGA spectrum a strong band at 1746 cm^{-1} is present, which can be assigned to stretching vibration of carbonyl groups. There are also bands between 1300 and 1150 cm^{-1} originating from asymmetric and symmetric C-C(=O)-O stretching vibrations [3,13].

In the spectrum of PEG characteristic bands are visible: at 3400 cm^{-1} due to stretching vibrations of water molecules, at around 2880 cm^{-1} and in the range of 1450–1240 cm^{-1} due to stretching and deformational vibrations of hydrocarbon in CH_2 groups, respectively. Moreover, bands in the range of 1000–1200 cm^{-1} are attributed to stretching vibrations of CO and COC groups. At lower wavenumbers in the range of 840–940 cm^{-1} bands assigned to bending vibrations of hydrocarbon groups in CH_2 are observed [3,14].

In the spectrum of POx there are bands at 1130 cm^{-1} and 1621 cm^{-1}. The band in the range 1700-1600 cm^{-1} is characteristic for poly(2-oxazolines) and is due to stretching vibrations of C=O and C-N groups [15].

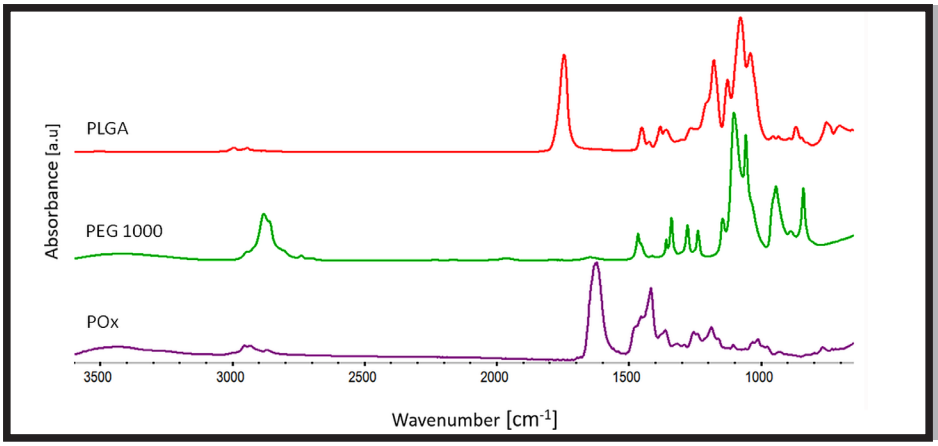

FIG. 1. FTIR-ATR spectra of main ingredients: PLGA, PEG 1000, and POx.

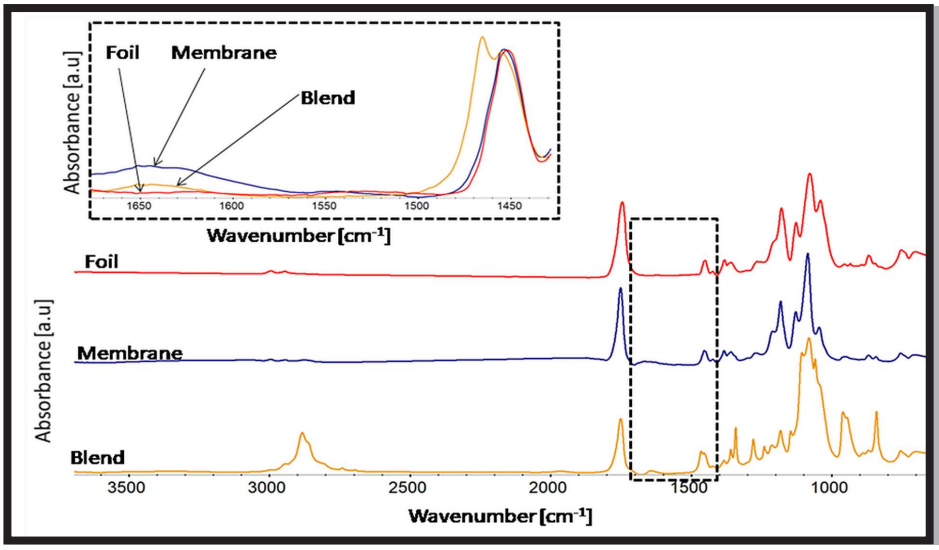

FIG. 2. FTIR-ATR spectra of PLGA foil (Foil), PLGA-POx membrane (Membrane), and PLGA-POx-PEG blend (Blend). In the insert respective spectra in the range of 1400-1690 cm^{-1} are shown for better visualization of differences.

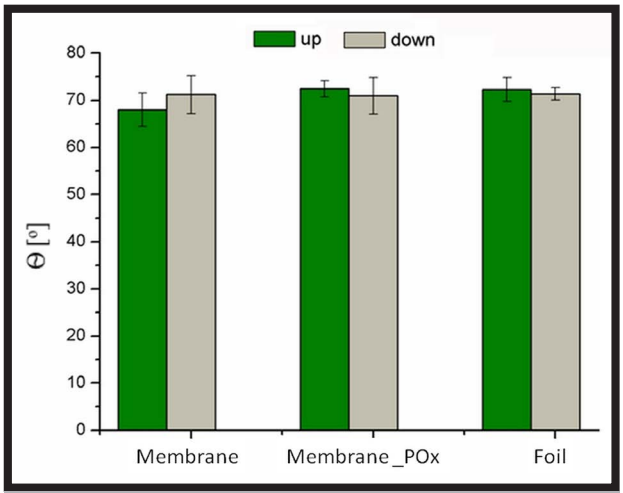

FIG. 3. Water contact angle values of PLGA membrane, PLGA membrane modified with POx, and PLGA foil: up / down – surfaces in contact with air / glass during preparation. No significant differences according to ANOVA.

As it is shown in FIG. 2 PLGA-POx-PEG blend contains all peaks characteristic for all ingredients: at 1746 cm^{-1} for PLGA, at around 2880 cm^{-1} for PEG, and at around 1620 cm^{-1} for poly(2-oxazolines). The membrane contains all bands characteristic for PLGA foil (strong band at 1746 cm^{-1}, due to stretching vibration of carbonyl groups and bands between 1300 and 1150 cm^{-1} from asymmetric and symmetric C-C(=O)-O stretching vibrations) [9]. The peaks of medium intensity at 2950 and 1370 cm^{-1} are attributed to C-H stretching and bending modes in PLGA structure, respectively. Moreover, a weak and wide band at around 1620 cm^{-1} from C=O and C-N stretching vibrations, which is characteristic for poly(2-oxazoline) structure is visible [15]. This band is not observed in the spectrum PLGA foil, what is an indirect proof that POx is immobilized on the surface of the membranes.

The results of wettability of PLGA membrane, PLGA membrane modified with POx and PLGA foil, both lower and upper surfaces, i.e. being in contact with glass and air during preparation are shown in FIG. 3. It is apparent that all analysed materials are hydrophilic with the water contact angle of about 70°. No significant differences were found between all studied materials.

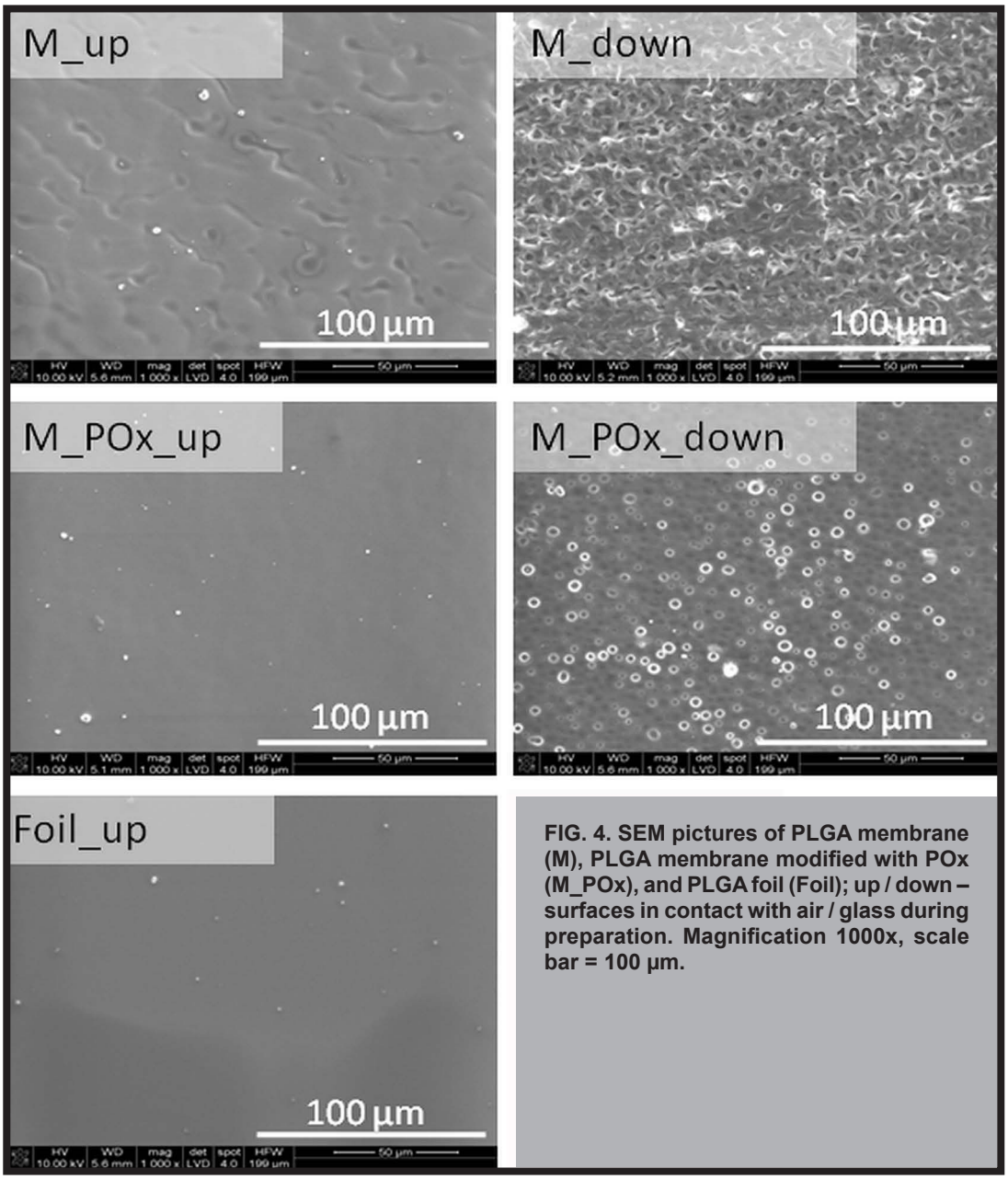

FIG. 4. SEM pictures of PLGA membrane (M), PLGA membrane modified with POx (M_POx), and PLGA foil (Foil); up / down – surfaces in contact with air / glass during preparation. Magnification 1000x, scale bar = 100 µm.

SEM results (FIG. 4) show that the air-cured (M_up, M_POx_up) and glass-cured (M_down, M_POx_down) surfaces of the membranes have different microstructure. Air-cured surfaces are smoother and non-porous, while glass-cured are porous. Thus, asymmetric membranes were obtained. Interestingly, the presence of POx in the membrane resulted in reduction in roughness on the air-cured surface and reduction in pore size and pore number on the glass-cured surface. PLGA foil was the smoothest among all studied materials.

To verify if PLGA membranes produced were compatible with cells *in vitro*, viability and morphology of MG-63 osteoblast-like cells were studied. The cells were cultured on both surfaces of two membranes: with and without POx and reference PLGA foil for 24 and 72 h (FIG. 5). The viability of the cells cultured for 24 h on all the membranes was the same or higher as compared to cell viability on control foil. The viability of the cells cultured for 72 h on all the membranes was significantly higher as compared to control foil. This suggests that the PLGA membranes are cytocompatible with model osteoblasts and that presence of POx does not have a negative impact on cells.

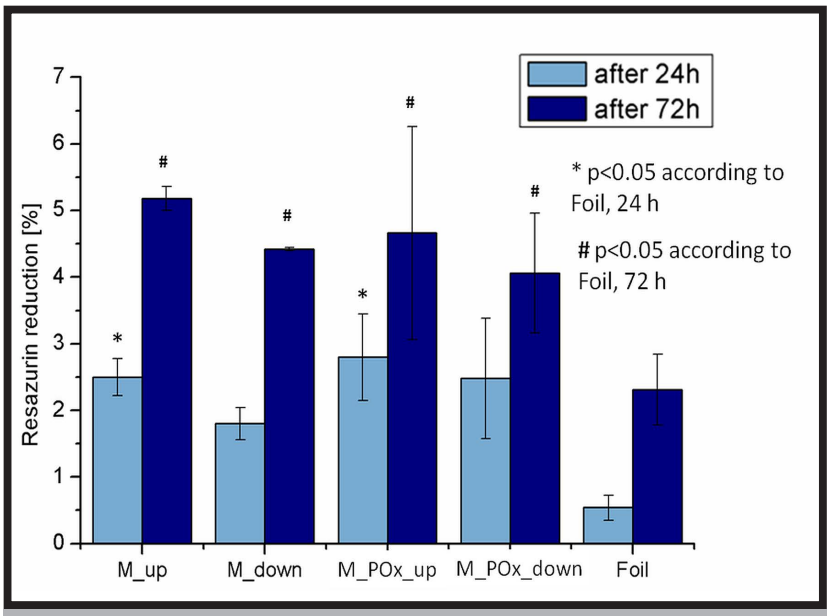

FIG. 5. MG-63 cell viability measured by resazsurin reduction for PLGA membrane (M), PLGA membrane modified with POx (M_POx), and PLGA foil (Foil); up / down – surfaces in contact with air / glass during preparation. Statistical significance according to ANOVA at p< 0.05.

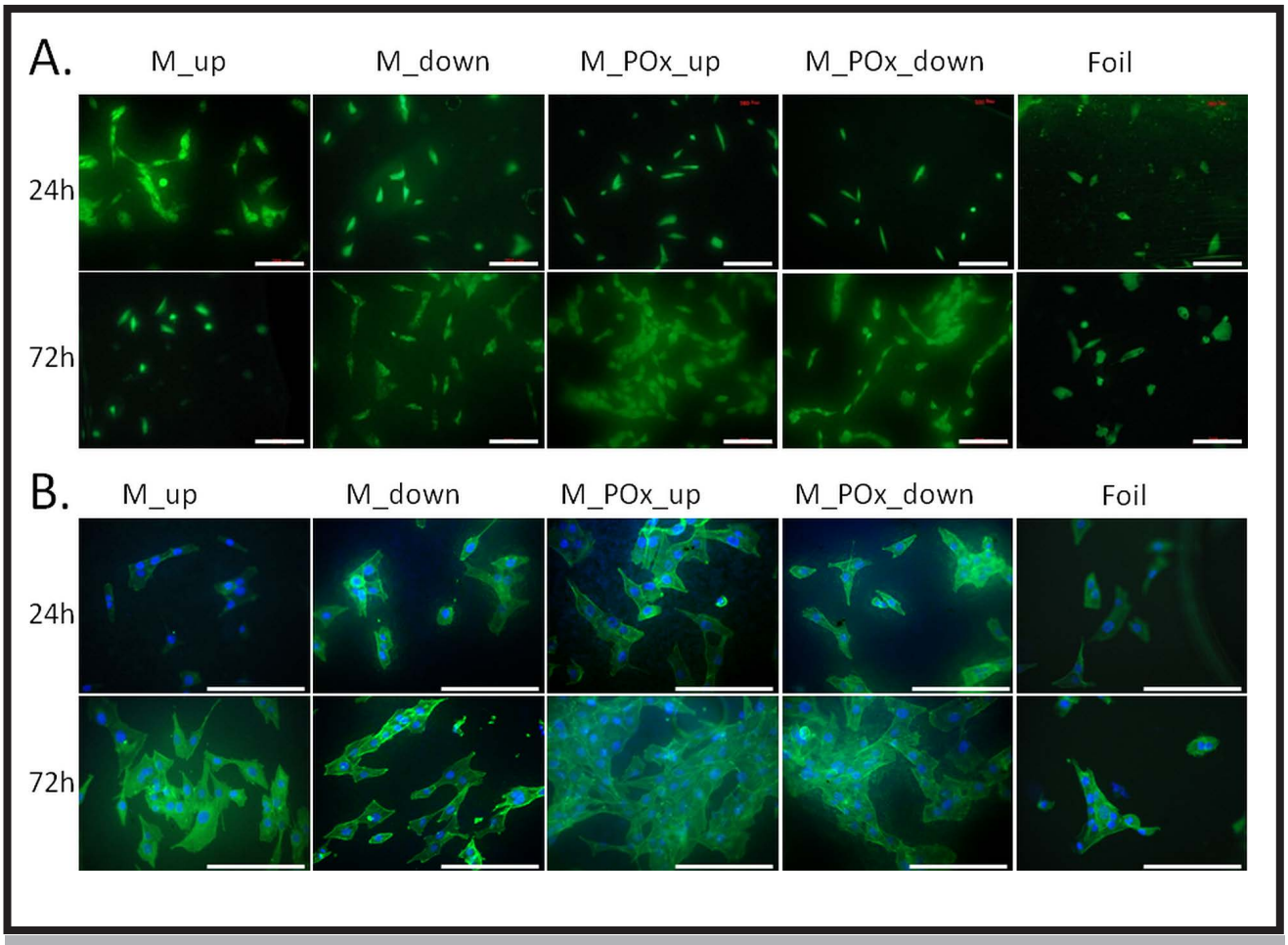

FIG. 6. Morphology of MG-63 cells cultured on PLGA membranes (M), membranes modified with POx (M_POx), and foil; up / down – surfaces in contact with air / glass during preparation. Cells stained live/dead (A) and for phalloidin/DAPI (B). Scale bar = 100 µm.

Microscopic observations of MG-63 cells after live/dead staining show that all cells on 24 h and 72 h of culture were stained green, i.e. were alive; no dead cells i.e. stained red were found (FIG. 6 A). Cells were homogenously distributed and their morphology was similar to that on PLGA foil. The number of adhering cells after 72 h looked higher on the membranes modified with POx.

Cells cultured on all membranes were better spread and had better developed actin fibres as compared to cells cultured on foils for 24 h (FIG. 6 B). After 72 h cells cultured on membranes with POx showed the most flattened morphology with intensively stained cytoskeleton.

Conclusions

In this study, we developed a method of manufacturing of porous asymmetric PLGA membranes modified with POx. The membranes were obtained by phase separation and preferential adsorption of POx molecules at the interface PLGA-POx-PEG followed by PEG leaching. Surface modification of PLGA with POx was confirmed by FTIR-ATR, by the presence of a band at about 1620 cm^{-1}, attributed to C=O and C-N stretching vibrations from poly(2-oxazolines), which was not found in the spectra of PLGA nor PEG.

Addition of POx influenced topography of the membranes, by decreasing average pore size on the glass-cured surface of the membrane and decreasing surface roughness of the air-cured surface of the membranes. Interestingly, the addition of POx did not influence membranes' wettability.

All membranes were found cytocompatible with osteoblast-like cells. Presence of POx resulted in better cell adhesion as shown by microscopic studies after fluorescence staining for nuclei and cytoskeleton actin fibers.

To sum up, one-step phase separation process between PLGA, POx, and PEG, dissolved in DCM followed by drying and PEG leaching resulted in cytocompatible, asymmetric PLGA membranes, which might be considered for guided tissue regeneration technique in periodontology and in bone tissue engineering.

Acknowledgments

The authors thank Prof. P. Dobrzyński (CPCM, PAS, Zabrze, Poland) and Prof. R. Jordan (TU, Dresden, Germany) for providing PLGA and POx, respectively. This study was supported from Interfaculty Environmental Doctoral Studies (FCB) at the Faculty of Materials Science and Ceramics, AGH University of Science and Technology.

References

[1] Linde A., Alberius P., Dahlin C., Bjurstam K., Sundin, Y.: Osteopromotion: A Soft-Tissue Exclusion Principle Using a Membrane for Bone Healing and Bone Neogenesis. Journal of Periodontology, 64(11s) (1993) 1116-1128. https://doi.org/10.1902/jop.1993.64.11s.1116

[2] Gentile P., Chiono V., Carmagnola I., Hatton, P.V.: An overview of poly(lactic-co-glycolic) Acid (PLGA)-based biomaterials for bone tissue engineering. International Journal of Molecular Sciences 15(3), (2014) 3640-3659. https://doi.org/10.3390/ijms15033640

[3] Krok M., Pamuła E.: Poly(L-lactide-co-glycolide) Microporous Membranes for Medical Applications Produced with the Use of Polyethylene Glycol as a Pore Former. J Applied Polymer Science 125 (2012) E187-E199.

[4] Bartold P.M., Gronthos S., Ivanovski S., Fisher A., Hutmacher D.W.: Tissue engineered periodontal products. Journal of Periodontal Research 51(1) (2016) 1-15. https://doi.org/10.1111/jre.12275

[5] Pa Z., Ding J.: Poly(lactide-co-glycolide) porous scaffolds for tissue engineering and regenerative medicine. Interface Focus 2(3) (2012) 366-377. https://doi.org/10.1098/rsfs.2011.0123

[6] Zhang R., Ma P.X.: Poly(alpha-hydroxyl acids)/hydroxyapatite porous composites for bone-tissue engineering. I. Preparation and morphology. Journal of Biomedical Materials Research 44 (1999) 446-455.

[7] Battistella E., Varoni E., Cochis A., Palazzo B., Rimondini L.: Degradable polymers may improve dental practice. Journal of Applied Biomaterials & Biomechanics 9(3) (2011) 223-231. https://doi.org/10.5301/JABB.2011.8867

[8] Datta S., Jutková A., Šrámková P., Lenkavská L., Huntošová V., Chorvát D., Miškovský P., Jancura D., Kronek J.. Unravelling the Excellent Chemical Stability and Bioavailability of Solvent Responsive Curcumin-Loaded 2-Ethyl-2-oxazoline-grad-2-(4--dodecyloxyphenyl)-2-oxazoline Copolymer Nanoparticles for Drug Delivery. Biomacromolecules 19 (2018) 2459-2471.

[9] Adams N., Schubert U.S.: Poly(2-oxazolines) in biological and biomedical application contexts. Advanced Drug Delivery Reviews, 59(15) (2007) 1504-1520. https://doi.org/10.1016/j.addr.2007.08.018

[10] Scharnweber D., Jordan R., Pamula E.: Oberflächenfunktionalisiertes Polymer für biologische Anwendungen und Verfahren zu dessen Herstellung, Patent DE 102013225772 B4, recieved 2016-11-14; published 2017-03-02.

[11] Dobrzynski P., Kasperczyk J., Janeczek H., Bero M.: Synthesis of Biodegradable Copolymers with the Use of Low Toxic Zirconium Compounds. 1. Copolymerization of Glycolide with L-Lactide Initiated by $Zr(Acac)_4$. Macromolecules 34 (2001) 5090-5098.

[12] Luxenhofer R., Schulz A., Roques C., Li S., Bronich T.K., Batrakova E.V., Jordan R., Kabanov A.V.: Doubly amphiphilic poly(2--oxazoline)s as high high-capacity delivery systems for hydrophobic drugs. Biomaterials 31 (2010) 4972-4979.

[13] Pamuła E., Błazewicz M., Paluszkiewicz C., Dobrzyński P.: FTIR study of degradation products of aliphatic polyesters-carbon fibres composites. Journal of Molecular Structure 596(1-3) (2001) 69-75. https://doi.org/10.1016/S0022-2860(01)00688-3

[14] Souza Júnior F.G. de, Cerruti R., Pinto J.C., Peña L., Saez V., Ramón J.A., Fernandes E.: Influence of PLGA and PLGA-PEG on the dissolution profile of oxaliplatin. Polímeros 26(2) (2016) 137-143. https://doi.org/10.1590/0104-1428.2323

[15] Macgregor-Ramiasa M.N., Cavallaro A.A., Vasilev K.: Properties and reactivity of polyoxazoline plasma polymer films. Journal of Materials Chemistry 3(30) (2015) 6327-6337. DOI: 10.1039/c5tb00901d

WYTRZYMAŁOŚĆ ZMĘCZENIOWA WIELOFUNKCYJNEJ RESORBOWALNEJ PŁYTKI KOMPOZYTOWEJ W SYMULOWANYCH WARUNKACH BIOLOGICZNYCH

Karol Gryń*, Barbara Szaraniec, Jan Chłopek

AGH Akademia Górniczo-Hutnicza,
Wydział Inżynierii Materiałowej i Ceramiki,
Katedra Biomateriałów i Kompozytów,
Al. Mickiewicza 30, 30-059 Kraków
*e-mail: kgryn@agh.edu.pl

Streszczenie

Artykuł jest kolejną częścią prezentującą wyniki badań mechanicznych wielofunkcyjnych resorbowalnych płytek zespalających. Testy dotyczyły wyznaczenia wytrzymałości zmęczeniowej płytek zespalających w warunkach symulujących rzeczywiste warunki pracy. Określenie tego parametru, zwłaszcza w elementach poddawanych obciążeniom zmiennym w czasie, jest bardzo ważne ze względu na możliwość wystąpienia w materiale zmian strukturalnych np.: umocnienia odkształceniowego czy rozwoju defektów prowadzących do zniszczenia elementu. Materiały kompozytowe o osnowie polimerowej modyfikowane cząstkami ceramicznymi są stosunkowo czułe na tego typu obciążenia.

Kolejnym aspektem, który musi być uwzględniony przy opisie i charakterystyce mechanicznej przedmiotowych implantów jest środowisko, w jakim się one docelowo znajdą. Temperatura, pH oraz skład chemiczny to czynniki bezpośrednio wpływające na sposób i tempo degradacji polimeru resorbowalnego. Degradacja z kolei wpływa na charakterystyki wytrzymałościowe osłabiając materiał.

W prezentowanych badaniach zastosowano modelowe zespolenie, w którym rolę odłamów kostnych pełniły specjalnie przygotowane bloczki z PMMA, do których za pomocą śrub metalowych przymocowana była testowana płytka. Tak przygotowany układ mocowano w maszynie zmęczeniowej i poddawano cyklicznemu rozciąganiu. Zastosowano dwa warianty badania: pierwsze, gdzie modelowe zespolenie obciążano „na sucho" bez obecności płynów symulujących środowisko biologiczne; i drugi, gdzie modelowe zespolenie umieszczano w zamkniętym zbiorniku, wypełnionym płynem symulującym środowisko biologiczne. Jako medium zastosowano płyn Ringera podgrzewany do temperatury ~37°C.

Na podstawie otrzymanych wyników stwierdzono, że płytki badane „na sucho", cechowały się inną charakterystyką niż płytki wystawione na oddziaływanie symulowanego środowiska biologicznego.

Słowa kluczowe: *płytka zespalająca, implant wielofunkcyjny, symulowane środowisko biologiczne, wytrzymałość zmęczeniowa, czas życia*

[Inżynieria Biomateriałów 147 (2018) 21-30

FATIGUE STRENGTH TESTS OF MULTIFUNCTIONAL RESORBABLE COMPOSITE PLATES IN SIMULATED BIOLOGICAL CONDITIONS

Karol Gryń*, Barbara Szaraniec, Jan Chłopek

AGH University of Science and Technology,
Faculty of Materials Science and Ceramics,
Department of Biomaterials and Composites,
Al. Mickiewicza 30, 30-059 Krakow, Poland
*e-mail: kgryn@agh.edu.pl

Abstract

The article is part of a series of publications presenting the results of mechanical tests of multifunctional resorbable fixation plates. Tests were conducted on prototype plates in conditions simulating natural biological environment. The examinations were meant to assess the so-called "implant working time" or fatigue strength of the fixation plates. This parameter is particularly important in the case of elements subjected to time-varying loads due to the possibility of alterations to the material structure, strain strengthening or development of defects leading to the implant failure.

Composite materials consisting in a polymer matrix modified with ceramic particles are quite sensitive to variable loads. Moreover, the complex geometry of the tested plates makes them more vulnerable to destruction with the critical cross-sections located at the fixing holes. Another key aspect is the biological environment where the implants will perform their functions. The temperature, pH and chemical composition are factors directly affecting the way and rate of degradation of the resorbable polymer. Degradation affects the strength characteristics, obviously weakening the material.

The tests were performed on a model composed of PMMA blocks playing the role of bones with the tested plate attached with metal screws. The model was mounted in a fatigue machine and subjected to cyclic stretching. Two variants of the examinations were performed. Firstly, the model was tested in "dry" conditions; secondly - in a closed container filled with fluids simulating the biological environment (the Ringer's solution heated to ~37°C used as the medium).

The results revealed that the plates tested in "dry" conditions were endowed with different characteristics as compared to the plates exposed to the simulated biological environment.

Keywords: *fixation plate, osteosynthesis, multifunctional implant, simulated biological environment, fatigue strength, working time*

[Engineering of Biomaterials 147 (2018) 21-30]

Wprowadzenie

Zastosowanie konwencjonalnej płytki w zespoleniu odłamów kostnych ma na celu zbliżenie ich do siebie oraz stabilne unieruchomienie [1-3]. Dąży się do odtworzenia ciągłości złamanej kości oraz przywrócenia jej funkcji. Opracowany resorbowalny implant jest nowatorski ze względu na swoją wielofunkcyjność i biodegradowalność [3-7]. Jego idea zakłada nie tylko trwałą mechaniczną stabilizację zespolenia, ale również kontrolowane, zwiększające się w czasie przenoszenie obciążeń mechanicznych z implantu na odbudowującą się tkankę kostną. Jednocześnie, wraz z degradacją osnowy polimerowej, mają się uwalniać z implantu nanocząstki ceramiczne poprawiające i przyspieszające naturalne procesy kościotwórcze [3,4]. Procesy degradacji, jakim podlegają w organizmie polimery resorbowalne, są ściśle związane m.in. z oddziaływaniem płynów ustrojowych oraz podwyższoną temperaturą [3-6]. Dodatkowo, w zależności od lokalizacji leczonego miejsca, płytka może być poddana różnym stanom naprężeniowo-odkształceniowym [7,11-14].

W celu zbadania jednoczesnego wpływu zmiennych obciążeń oraz środowiska biologicznego na czas życia implantu, przeprowadzono badania zmęczeniowe modelowego zespolenia przy użyciu płytek typu I wykonanych z polimeru resorbowalnego PLA oraz kompozytu PLA modyfikowanego bioceramicznymi proszkami TCP i HAp. Testy prowadzono w warunkach symulujących warunki pracy implantu (skład chemiczny, pH, temperatura). Zastosowano schemat cyklicznego jednoosiowego rozciągania w obecności ogrzanego płynu symulującego środowisko biologiczne.

Materiały i metody

Płytki zespalające

Do wytworzenia płytek zespalających użyto opracowane wcześniej kompozyty [15] składające się z polimerowej matrycy modyfikowanej cząstkami bioceramicznymi. Wykorzystano amorficzny polimer resorbowalny poli(L-laktyd) (PLA Ingeo 3251D, Nature Works LLC USA), do którego wprowadzono odpowiednią ilość (nieprzekraczającą sumarycznie 8% wag.) mikrometrycznego proszku fosforanu trójwapnia β-TCP (Chema Elektromet) oraz nanometrycznego hydroksyapatytu HAp (Chema Elektromet). Oba proszki posiadały dopuszczenie do zastosowań medycznych. Większe udziały objętościowe dodatków powodowały zatykanie się dyszy wtryskarki zatrzymując proces wtrysku.

Prototypy implantów wytworzono przy pomocy wtryskarki pionowej Multiplas V4-S-15N wyposażonej w ślimakowy układ uplastyczniająco-homogenizujący. Granulat polimerowy wraz z dodatkami bioceramicznymi zasypano do pojemnika wtryskarki. Po ogrzaniu wsadu do temp. 160°C homogenizowano go poprzez mieszanie ślimakiem wtryskarki. Tak przygotowany materiał wtryskiwano do formy. Dane technologiczne zamieszczono w TABELI 1.

Introduction

A conventional plate is used to bring together and immobilize bone fragments in case of bone fractures. Its function is to recreate the continuity of the broken bone and restore its function [1-3]. The developed resorbable implant is innovative due to its multifunctionality and biodegradability [3-7]. The concept assumes not only permanent mechanical stabilization but also controlled and gradually increasing transmission of mechanical loads from the implant to the reconstructing bone tissue. Simultaneously, while the polymer matrix is degrading, ceramic nanoparticles which improve and accelerate natural osteogenic processes are being released from the implant [3,4]. Implanted resorbable polymers undergo degradation processes due to the influence of body fluids and elevated temperature [3-6]. Additionally, the fixation plate is subjected to various stress-strain loads depending on the location of the fracture [7,11-14].

Fatigue tests of the model were performed to assess the combined effect of variable loads and the biological environment on the implant's working time. A few types of plates were designed for the examinations. The type I plate was based on resorbable PLA and PLA modified with bioceramic TCP and HAp powders. The tests were performed in conditions simulating the implant's working conditions (chemical composition, pH, temperature). A cyclic uniaxial stretching diagram was used in the presence of heated fluid simulating the biological environment.

Materials and Methods

Fixation plates

The previously developed composites [15] consisting of a polymer matrix modified with bioceramic particles were used to make the fixation plates. An amorphous poly (L-lactide) resorbable polymer (PLA Ingeo 3251D, Nature Works LLC USA) was enriched with an appropriate amount (not more than 8wt%) of the β-TCP tricalcium phosphate powder (Chema Elektromet) and HAp nanoparticle hydroxyapatite powder (Chema Elektromet). Higher content of powders makes injection moulding process impossible due to injection nozzle clogging. Both powders were approved for medical use. Implant prototypes were created using a Multiplas V4-S-15N vertical injection moulder equipped with a screw plasticizing-homogenizing system. Technological data is provided in TABLE 1.

The four-hole plates characterized by the length of 29 mm, width 7 mm, thickness 2 mm, bore diameter 3 mm and the conical socket for the fastening screw head were prepared for the tests from the following materials: the reference samples were pure polymer plates, i.e. polylactide (PLA) while the composite samples were based on PLA and bioceramic additives - TCP and HAp (PLA/TCP/HAp). Polymer granulate combined with bioceramic modifiers was applied to the heating chamber of the injection moulding machine.

TABELA 1. Parametry technologiczne otrzymywania (wtrysku) czterootworowych mini płytek I.
TABLE 1. Technological parameters of injection moulding process of the four-hole I-shaped plates fabrication.

Materiał Material	Temperatura / Temperature [ºC]			Ciśnienie Pressure* [kg/cm²]	Przepływ Flow [%]	Czas wtrysku Injection time [s]	Czas chłodzenia Cooling time [s]
	Strefa1 Zone 1	Strefa 2 Zone 2	Strefa 3 Zone 3				
PLA	160	165	168	80	60	5	10
PLA/TCP/HAp	165	170	175	80	60	5	15

** ciśnienie w hydraulicznym siłowniku ślimakowo-tłokowym wtryskarki*
** the pressure in the hydraulic system of injection molding machine (perpetual screw)*

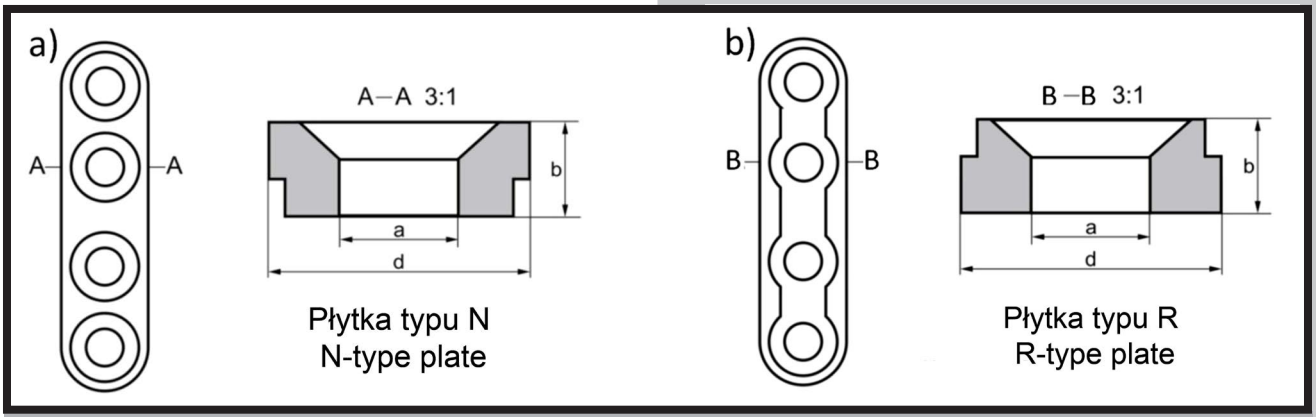

RYS. 1. Prototypowa płytka i jej przekrój poprzeczny: a) typ N – żeberko wzmacniające na dolnej powierzchni; b) typ R – żeberko wzmacniające na górnej powierzchni.
FIG. 1. Two types of prototypes of the plate and their cross-section: a) N-type with strengthening rib on the bottom side; b) R-type with strengthening rib on the upper side.

Do badań przygotowano płytki czterootworowe o kształcie litery I (dł. 29 mm, szer. 7 mm, gr. 2 mm, średnica otworu 3 mm, stożkowe gniazdo pod łeb śruby mocującej) z następujących materiałów: próbki odniesienia stanowiły płytki z czystego polimeru tj. polilaktydu (PLA); próbki kompozytowe bazowały na osnowie z PLA oraz dodatkach bioceramicznych tj: TCP i HAp (PLA/TCP/HAp). Ponieważ nie istnieją wytyczne dotyczące projektowania kształtu kompozytowych płytek zespalających, zaadoptowano i odpowiednio zmodyfikowano geometrię czterootworowej płytki zespalającej wykonanej ze stali 316L (postępowanie jest przedmiotem zgłoszenia patentowego). Przygotowany projekt płytki uwzględniał zastosowanie tzw. żeberka wzmacniającego. Miało ono na celu poprawienie charakterystyk mechanicznych i redukcję przekroju, a zlokalizowanie go na dolnej stronie płytki zmniejszyć powierzchnię jej kontaktu z kością, czyniąc oddziaływanie mniej inwazyjnym. Aby zweryfikować przyjęte założenia projektowe z każdego rodzaju materiału wykonano dwa warianty geometryczne różniące się między sobą położeniem żeberka wzmacniającego (RYS. 1). Zastosowano następujące oznaczenia: płytka I typu N posiadała żeberko wzmacniające po stronie mocowania do odłamu kostnego (RYS. 1a), natomiast w płytce I typu R po stronie przeciwnej (RYS. 1b).

Badania zmęczeniowe

W celu wyznaczenia wytrzymałości zmęczeniowej implantów przeprowadzono badania cyklicznego rozciągania zgodne z normą PN-EN ISO 527-1:2012 [16]. Aby uzyskać dane potrzebne do zaprojektowania testów zmęczeniowych, konieczne było wyznaczenie charakterystyk wytrzymałościowych płytek w próbie statycznego jednoosiowego rozciągania. Przeprowadzono je zgodnie z normą PN-EN ISO 527-1:2012. Badania zrealizowano na maszynie wytrzymałościowej Zwick 1435, sprzężonej z oprogramowaniem TextExpet v8.1. Prędkość przesuwu trawersy ustalono na 20 mm/min. Na podstawie uzyskanych wyników określono: odkształcenie przy maksymalnej sile ε_{Fmax}, wytrzymałość na rozciąganie R_m oraz moduł Younga E (TABELA 2).

It was heated up to 160°C and homogenized with rotating screw. After homogenisation material was injected into the mold.

There are no designing guidelines for composite plates for osteosynthesis. That is why standard directions for designing the metal four-holes plate were adapted and modified (patent pending). The design of the four-hole composite plate included so called strengthening rib. It was designed for increasing the mechanical properties of the plate, reducing its dimensions and also, when strengthening rib is located on the bottom part of the plate the contact surface between bone and plate is smaller. To verify design assumptions two types of fixation plates were made from each type of the material, differing in the position of the reinforcing rib (FIG. 1). The following markings were used: the N-shaped plate had a reinforcing rib on the bottom side (FIG. 1a), whereas in the R-shaped plate on the upper side (FIG. 1b).

Fatigue strength tests

In order to determine the fatigue strength of the implants, cyclic extension tests were carried out in accordance with the PN-EN ISO 527-1: 2012 standard [16]. To obtain the data needed to design fatigue tests, it was necessary to determine the strength characteristics of the plates in the static uniaxial stretching test. These were performed in accordance with the PN-EN ISO 527-1: 2012 standard. The research was carried out on a Zwick 1435 testing machine, coupled with the TextExpet v8.1 software. The traverse speed was set at 20 mm/min. On the basis of the obtained results, the following values were determined: strain at maximum force ε_{Fmax}, tensile strength R_m and Young's modulus E (TABLE 2).

TABELA 2. Zestawienie wyników próby statycznego jednoosiowego rozciągania. Płytki mocowano do bloczków z PMMA momentem dokręcającym wynoszącym: M_{dokr} = 60% M_{max}.
TABLE 2. Uniaxial tensile test results. Plates were fixed to the PMMA blocks with suitable tightening torque: M_t = 60% M_{max}.

Wielkość Parameter		Płytka / Plate		
			PLA	PLA/TCP/HAp
Wytrzymałość na rozciąganie Tensile strength R_m [MPa]		N	45.83 ± 1.62	45.51 ± 2.2
		R	38.53 ± 1.64	47.74 ± 3.03
Moduł Younga Young's Modulus E [GPa]		N	6.28 ± 0.36	6.21 ± 0.54
		R	6.16 ± 0.69	5.98 ± 0.63
Wydłużenie przy max. sile Maximal elongation ε_{Fmax} [mm]		N	1.53 ± 0.05	1.58 ± 0.23
		R	1.3 ± 0.18	1.39 ± 0.4

TABELA 3. Wartości amplitudy cyklicznego rozciągania próbek przyjęte w testach zmęczeniowych.
TABLE 3. Cyclic deformation values used in fatigue tensile tests.

		PLA			PLA/TCP/HAp		
Wartość odkształcenia (amplitudy) zastosowanego w testach cyklicznego rozciągania odniesiona do ε_{Fmax} Cyclic deformation values (amplitude) used in fatigue tensile tests ε_{Fmax}		50%	40%	30%	50%	40%	30%
Wartość odkształcenia (amplitudy) zastosowanego w testach cyklicznego rozciągania [mm] Cyclic deformation values (amplitude) used in fatigue tensile tests [mm]	N	0.77	0.61	0.46	0.79	0.63	0.47
	R	0.65	0.52	0.39	0.70	0.68	0.42

Wytrzymałość zmęczeniowa „na sucho”

Testy te miały na celu zbadanie wpływu na przygotowane płytki cyklicznie zmiennych naprężeń rozciągających. Wartości R_m oraz ε_{Fmax} stanowiły dane wyjściowe, na podstawie których wyznaczono amplitudę odkształceń zastosowanych w badaniach zmęczeniowych. Przyjęto, że ich wartości wyniosą kolejno: 50%, 40% i 30% odkształcenia przy maksymalnej sile. Wartości liczbowe wyrażone w milimetrach zamieszczono w TABELI 3.

Modelowe zespolenie czyli płytki przykręcone do bloczków PMMA odpowiednim momentem dokręcającym mocowano w uchwytach stanowiska do badań cyklicznego rozciągania (RYS. 2). Zastosowano częstotliwość rozciągania wynoszącą 700 cykli na minutę. Badanie trwało przez dziesięć tysięcy cykli lub do momentu stwierdzenia pierwszych oznak zniszczenia w postaci najmniejszych obserwowalnych gołym okiem pęknięć lub do zerwania płytki.

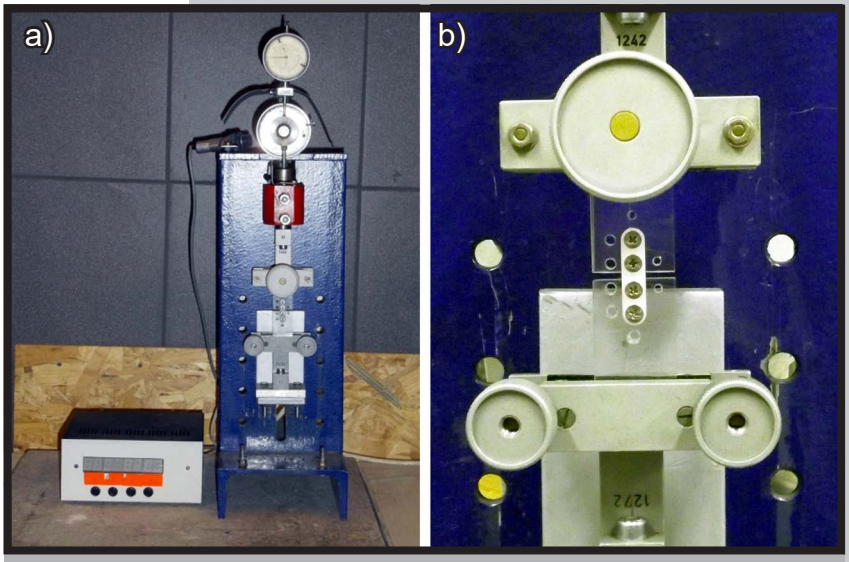

RYS. 2. a) Stanowisko do badań zmęczeniowych; b) Sposób mocowania modelowego zespolenia za pomocą kompozytowej płytki czterootworowej.
FIG. 2. a) Test stand for dynamic fatigue test; b) Fixation and orientation of the composite plate.

Wytrzymałość zmęczeniowa w symulowanych warunkach biologicznych

W celu zbadania jednoczesnego wpływu zmiennych obciążeń oraz środowiska biologicznego na czas życia implantu, przeprowadzono badania zmęczeniowe modelowego zespolenia w warunkach cyklicznego jednoosiowego rozciągania w obecności podgrzanego płynu Ringera (Baxter USA) symulującego warunki pracy implantu (skład chemiczny, pH, temperatura).

Do testów przygotowano specjalne stanowisko. Maszynę do badań zmęczeniowych doposażono w zamykaną szczelną komorę, pozwalającą na badanie modelowego zespolenia zanurzonego w sztucznym płynie fizjologicznym (RYS. 3). Układ zawierał również grzałkę z kontrolerem temperatury oraz dodatkowy zintegrowany zbiornik z pompą łopatkową. Badania prowadzono w temperaturze zbliżonej do temperatury ciała ludzkiego (~37°C) a wymuszony obieg medium (ciągły przepływ) zapewniał równomierny jej rozkład w całej objętości płynu.

Testy przeprowadzono zgodnie z obowiązującą normą PN-EN ISO 527-1: 2012. Częstotliwość zmiennego obciążenia realizowana na stanowisku wynosiła 700 cykli na minutę. Dla każdego rodzaju próbek ustawiono liczbę cykli na poziomie 10000 oraz amplitudę wynoszącą kolejno: 50%, 40% i 30% odkształcenia przy maksymalnej sile. Testy przerywano w chwili stwierdzenia pierwszych oznak zniszczenia w postaci najmniejszych obserwowalnych gołym okiem pęknięć lub w momencie przerwania ciągłości płytki. Nie sporządzono wykresów Wöhlera oraz nie wykonano obliczeń statystycznych ze względu na testowy charakter badań.

Fatigue tensile strength tests in “dry” conditions

The tests were aimed at investigating the influence of cyclically variable tensile stresses on the plates. The values of R_m and ε_{Fmax} were the output data serving as the basis for the strain amplitude used in fatigue tests. It was assumed that their values would be: 50%, 40% and 30% strain at maximum force. Numerical values expressed in millimeters are shown in TABLE 3.

The model of bone fixation, i.e. the plates bolted to the PMMA blocks with a suitable tightening torque, were mounted in the holders of the test stand for cyclic stretching (FIG. 2). A stretching frequency of 700 cycles per minute was applied. The test lasted for 10,000 cycles or until the first signs of damage were observed as the smallest crack visible to the naked eye or to breaking the plate.

Fatigue tensile strength in a simulated biological environment

In order to investigate the simultaneous effect of variable loads and the biological environment on the implant’s working time, fatigue tests were performed on a special test stand. The model was exposed to cyclic uniaxial stretching in the presence of heated Ringer’s solution (Baxter USA) simulating the implant’s working conditions (chemical composition, pH, temperature). The fatigue testing machine was equipped with a sealed chamber, allowing for the examination of the model immersed in an artificial physiological fluid (FIG. 3).

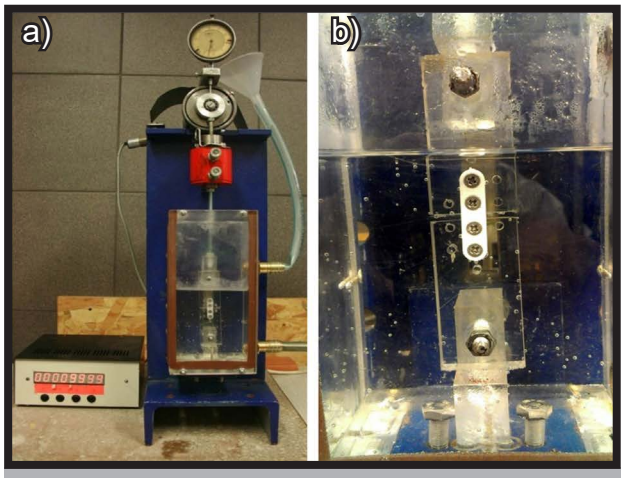

RYS. 3. a) Stanowisko do badań zmęczeniowych w symulowanym środowisku biologicznym. Widoczny specjalnie skonstruowany zbiornik na sztuczne płyny fizjologiczne; b) Widok modelowego zespolenia za pomocą płytki PLA/HAp/TCP.
FIG. 3. a) Test stand for dynamic fatigue test in biological simulated conditions with special tank/ reservoir for heated Ringer solution; b) Model of simulated osteosynthesis used in tests.

Wyniki i dyskusja

Wytrzymałość zmęczeniowa „na sucho”

Zaplanowano badanie próbek w trakcie 10000 cykli przy zastosowaniu trzech zakresów odkształcenia 50%, 40% i 30% ε_{Fmax}. Stwierdzono, że przy zastosowaniu amplitudy 50% ε_{Fmax} (ok. 0,7 mm) próbki z czystego polimeru PLA (zarówno typu N jak i R) ulegały zniszczeniu już po ok. 1500 cyklach, a ich destrukcja była całkowita (RYS. 4a). Wyraźnie widoczne były promieniste pęknięcia propagujące w kierunkach prostopadłych do siebie (RYS. 4b). Próbki pękały w sposób nagły, a charakter pękania był kruchy. Pojawiające się pęknięcia natychmiast propagowały i dochodziło do zerwania płytki. Z tego powodu niemożliwe było określenie momentu (ilości cykli), w którym pęknięcia się pojawiały. Po zmniejszeniu amplitudy do 40% ε_{Fmax} (ok. 0,55 mm) stwierdzono poprawę w zachowaniu się próbki. Przetrwała zaplanowany program 10000 cykli, jednakże po zdjęciu jej z uchwytów mocujących, w okolicy obu otworów (bliższego i dalszego), ujawniono zainicjowane pęknięcia, zaś na drugim końcu płytki, w okolicy dalszego otworu, stwierdzono pęknięcie całkowite (RYS. 4c). Po zmniejszeniu amplitudy rozciągania do 30% ε_{Fmax} (ok. 0,4 mm) i przeprowadzeniu 10.000 cykli nie stwierdzono oznak zniszczenia próbek wykonanych z czystego PLA. W TABELI 4 oraz na RYS. 5 przedstawiono zebrane wyniki.

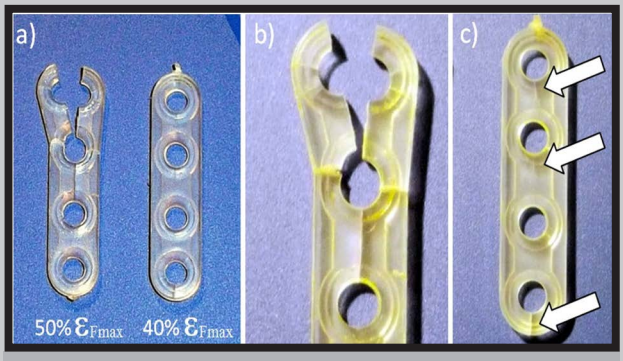

RYS. 4. Przykłady zniszczonych płytek z PLA po testach cyklicznego jednoosiowego rozciągania przy 50% i 40% ε_{Fmax}.
FIG. 4. Examples of destroyed PLA plates after dynamic uniaxial fatigue tests with 50% and 40% of ε_{Fmax}.

The designed system also included a heater with a temperature controller and an additional integrated tank with a vane pump. The tests were carried out at a temperature close to the temperature of the human body (~37°C) and the forced circulation of the medium (continuous flow) ensured its even distribution in the entire volume of liquid. The tests were carried out in accordance with the PN-EN ISO 527-1: 2012 standard. The frequency of variable load was 700 cycles per minute. The number of cycles was 10,000 and the amplitude of 50%, 40% and 30% strain at maximum force were set for each type of sample. The tests were terminated when the first signs of damage occurred, i.e. the smallest cracks were observable by the naked eye or when the continuity of the plate was interrupted. Wöhler charts were not prepared and no statistical calculations were made due to the test nature of the investigation.

Results and Discussion

Fatigue tensile strength in „dry” conditions

Sample testing was planned during 10,000 cycles using three strain ranges of 50%, 40% and 30% ε_{Fmax}. It was found the amplitude of 50% ε_{Fmax} (about 0.7 mm) caused the failure of the pure PLA sample (both N and R type) after about 1500 cycles and their destruction was complete (FIG. 4a). Prominent cracks propagating in directions perpendicular to each other were clearly visible (FIG. 4b). The sample cracked suddenly and the nature of the cracking was brittle. The cracks immediately propagated and the plate was ruptured, that is why it was not possible to determine the moment when the cracks appeared (an exact number of cycles). Having reduced the amplitude to 40% ε_{Fmax} (about 0.55 mm), the sample survived the planned 10,000 cycles.

TABELA 4. Wyniki próby cyklicznego rozciągania „na sucho”.
TABLE 4. Number of cycles for various values of cyclic deformation “dry” fatigue tensile tests.

		Rodzaje płytek / Plate types					
		PLA			PLA/TCP/HAp		
Wielkość cyklicznego odkształcenia, amplituda ε_{Fmax} Cyclic deformation values (amplitude) used in fatigue tensile tests ε_{Fmax}		50%	40%	30%	50%	40%	30%
Liczba cykli, przy których nastąpiło zniszczenie płytki Number of cycles for sample destruction	N	~1500	~10.000 Spękania Cracks	>10.000	~1700	~3500	>10.000
	R	~1000	~10.000 Spękania Cracks	>10.000	~3200	~4000	>10.000

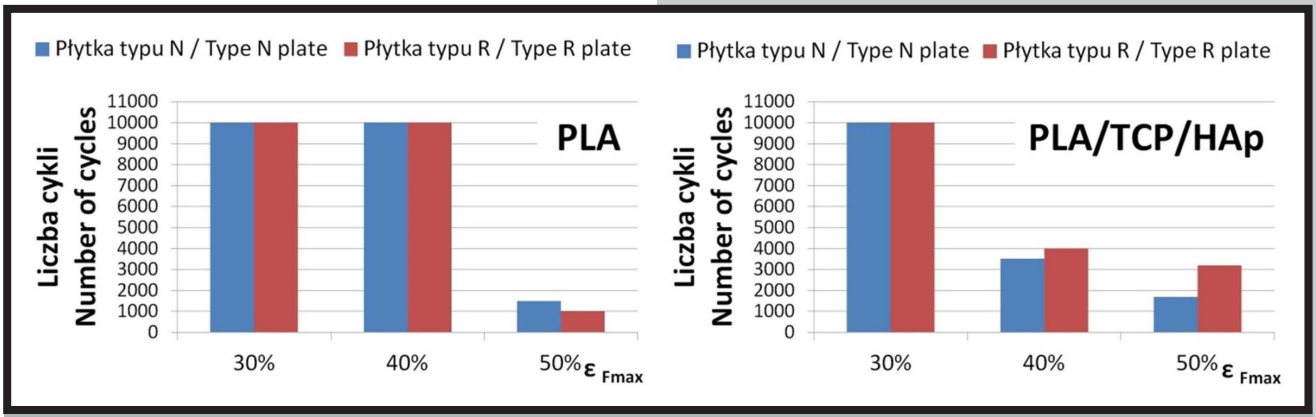

RYS. 5. Zestawienie wytrzymałości zmęczeniowej płytek czterootworowych „na sucho" przy różnych wartościach amplitudy.
FIG. 5. Comparison of fatigue strength for after "dry" testing of four-holes plate with various cyclic deformation values (amplitude).

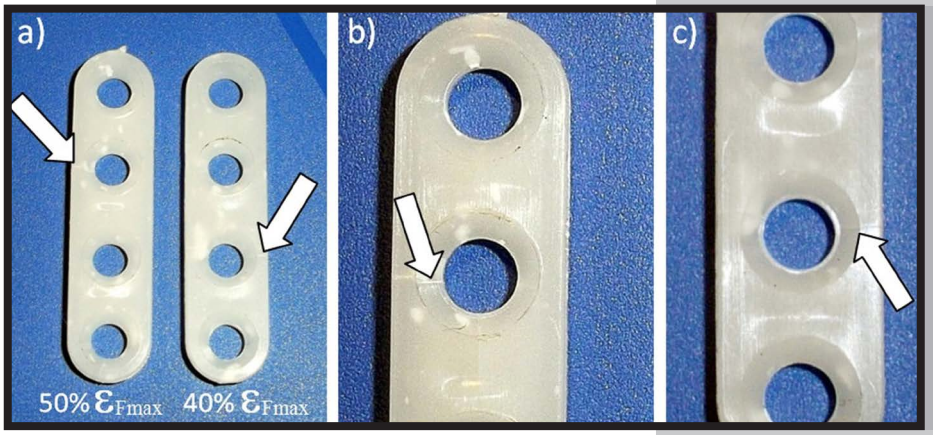

RYS. 6. Przykłady zniszczonych płytek z PLA/TCP/HAp po testach cyklicznego jednoosiowego rozciągania przy 50% i 40% ε_{Fmax}.
FIG. 6. Examples of destroyed PLA/TCP/HAp plates after dynamic uniaxial fatigue tests with 50% and 40% of ε_{Fmax}.

Analogiczny zestaw testów zastosowano podczas badania próbek z kompozytu PLA/TCP/HAp. Stwierdzono znacznie większą wytrzymałość płytek wykonanych z tego materiału w porównaniu z płytkami z czystego PLA. Przy zastosowaniu amplitudy o wartości 50% ε_{Fmax} (ok. 0,75 mm) po 3500 cykli stwierdzono pojawienie się jednego pęknięcia w okolicy otworu bliższego, jednak nie doszło do rozerwania płytki (RYS. 6a). Po obniżeniu wartości zadanego odkształcenia do 40% ε_{Fmax} (ok. 0,65 mm) po ok. 4000 cykli również stwierdzono pojawienie się pojedynczego pęknięcia, jednak i w tym przypadku spójność płytki nie została naruszona (RYS. 6b,c).

Po zmniejszeniu wartości odkształcenia do 30% ε_{Fmax} i przeprowadzeniu 10000 cykli nie stwierdzono oznak zniszczenia próbek wykonanych z PLA/TCP/HAp (RYS. 7).

Z uzyskanych wyników można wnioskować, że wprowadzenie do osnowy z PLA modyfikatorów w postaci proszków TCP i HAp zmieniło charakterystyki mechaniczne implantów. Zwiększył się zakres odkształceń sprężystych. Z drugiej zaś strony, podczas analizy procesu pękania płytek kompozytowych PLA/TCP/HAp stwierdzono niejednorodne rozmieszczenie cząstek w osnowie oraz obecność aglomeratów proszku (RYS. 8). Można zatem przypuszczać, że mogły one stanowić koncentratory naprężeń, a także zmniejszały efektywny – przenoszący naprężenia – przekrój próbki (RYS. 9) i to właśnie było prawdopodobną przyczyną inicjowania pęknięć.

However, after removing it from the mounting brackets, the initiated cracks were revealed near both holes (proximal and distal) and the total fracture was found at the other end of the plate (FIG. 4c). With the stretching amplitude reduced to 30% ε_{Fmax} (about 0.4 mm), the samples made of pure PLA showed no sign of destruction after 10,000 cycles. TABLE 4 and FIG. 5 show the collected results.

The same set of tests was used for the composite PLA/TCP/HAp samples. In comparison to the pure PLA plates, they revealed significantly higher strength values. With the amplitude of 50% ε_{Fmax} (about 0.75 mm), one crack appeared in the vicinity of the proximal hole after 3,500 cycles but the plate did not break (FIG. 6a). Having reduced the amplitude to 40% ε_{Fmax} (about 0.65 mm), a single crack was also found after about 4,000 cycles, yet the integrity of the plate was not affected (FIG. 6b, c). After further reduction of the deformation rate (to 30% ε_{Fmax}), no signs of destruction of the PLA/TCP/HAp samples were found after 10,000 cycles (FIG. 7).

The obtained results lead to the conclusion that introducing modifiers, such as TCP and HAp powders, into the PLA matrix has changed the mechanical characteristics of the implants. The range of elastic deformations has increased. On the other hand, the analysis of the cracking process of the composite PLA/TCP/HAp plates revealed the inhomogeneous distribution of particles in the matrix and the presence of powder agglomerates (FIG. 8). Therefore, one can assume that the agglomerates might have acted as stress concentrators and they also reduced the sample cross-section responsible for transferring the loads (FIG. 9), which was the likely cause of crack initiation.

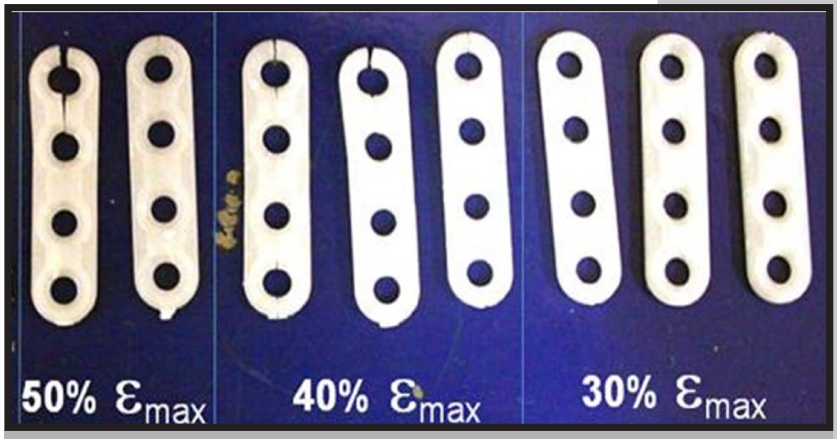

RYS. 7. Przykładowe próbki PLA/TCP/HAp po testach zmęczeniowych z różnymi wartościami odkształcenia. Brak oznak zniszczenia dla płytek badanych przy odkształceniu równym 30% ε_{Fmax}.
FIG. 7. Examples of destroyed PLA/TCP/HAp plates after dynamic uniaxial fatigue tests with various deformation rate. No signs of destruction were found in plates tested with the 30% ε_{Fmax} of the deformation rate.

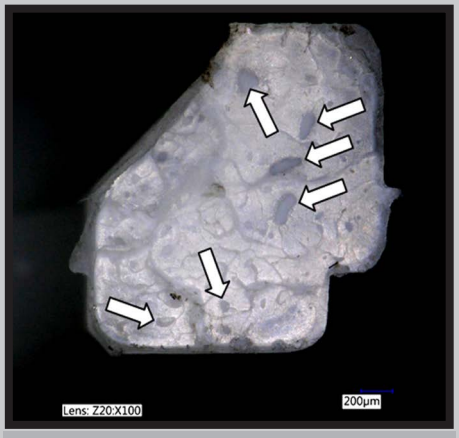

RYS. 9. Widok przełomu próbki typu N po zniszczeniu. Strzałkami zaznaczono aglomeraty proszków bioceramicznych (x100).
FIG. 9. Cross-section of the N-type plate. Arrows show TCP/HAp powder agglomerates (x100).

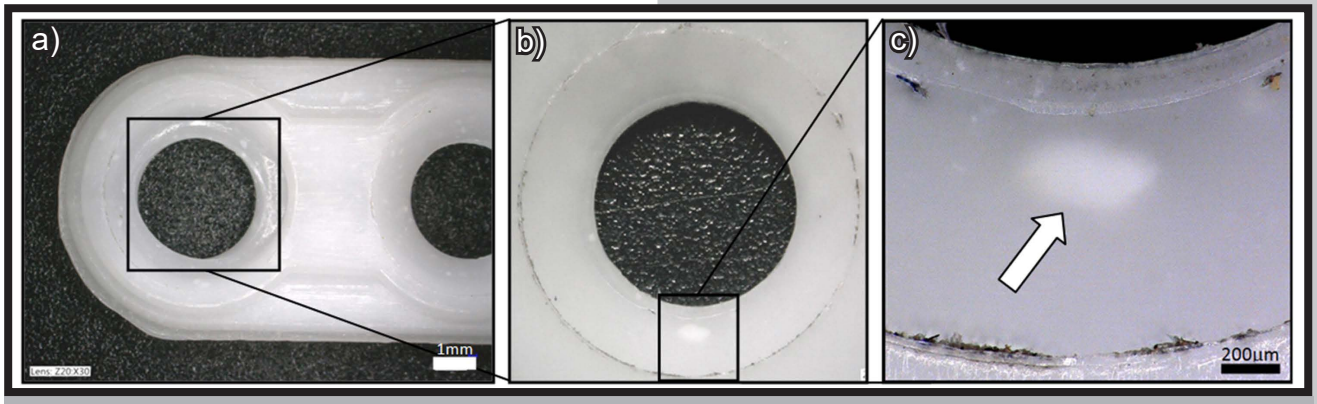

RYS. 8. Widoczne gołym okiem aglomeraty proszku TCP/HAp w okolicy otworu mocującego płytki. Powiększenie: a) x30, b) x50, c) x200.
FIG. 8. TCP/HAp powder agglomerates visible in the surrounding material of the plate's fixing hole. Magnification: a) x30, b) x50, c) x200).

Wytrzymałość zmęczeniowa w symulowanych warunkach biologicznych

Celem badań było sprawdzenie jaki jest wpływ symulowanego środowiska biologicznego na czas życia implantów podczas testów zmęczeniowych. Nie sporządzono wykresów Wöhlera oraz nie wykonano obliczeń statystycznych – badania testowe. Ze względu na wielofunkcyjny charakter implantów, do badań w symulowanych warunkach biologicznych wybrano płytki kompozytowe PLA/TCP/HAp. W pierwszej kolejności testom poddano płytki typu R, ponieważ z testów „na sucho" wynikało, że cechują się one większą wytrzymałością zmęczeniową niż płytki typu N. Początkowo zastosowana amplituda cyklicznych odkształceń wynosiła 50% odkształcenia maksymalnego, co stanowiło ok. 0,7 mm. Po umieszczeniu modelowego zespolenia w uchwytach maszyny zmęczeniowej i zalaniu płynem Ringera niemal natychmiast po uruchomieniu testu dochodziło do całkowitego zerwania próbek. Obniżenie wielkości amplitudy do 40% odkształcenia maksymalnego (ok. 0,47 mm) poprawiło sytuację, jednak wszystkie płytki uległy zniszczeniu przy niewielkiej liczbie cykli nieprzekraczającej pięciuset. Lepsze wyniki uzyskano po zmniejszeniu amplitudy do 30% ε_{Fmax} (ok. 0,42 mm), niemniej żadna próbka nie przetrwała 10000 cykli. Przy takiej wartości przeprowadzono również testy płytek typu N. Wyniki testów zamieszczono w TABELI 5.

Fatigue strength under simulated biological conditions

The fatigue tests were performed to assess the effects of the simulated biological environment on the working time of implants. Wöhler charts were not prepared and no statistical calculations were made. Due to the multifunctional character of implants, the PLA/TCP/HAp composite plates were selected for testing in simulated biological conditions. The R-type plates were tested first as the initial "dry" tests indicated their higher fatigue strength in comparison to the N-type plates. The applied amplitude of cyclic deformations was 50% of the maximum deformation, which was about 0.7 mm. After placing the model in the machine and flooding with Ringer fluid, the samples got destroyed immediately after the test started. Reducing the amplitude to 40% of the maximum deformation (about 0.47 mm) improved the situation, but all the plates were destroyed within a small number of cycles - not exceeding 500. Better results were obtained at the amplitude of 30% ε_{Fmax} (about 0.42 mm), however, no sample survived 10,000 cycles. At the 30% value, the N-type plates were also tested. The results of the tests are presented in TABLE 5.

Porównując uzyskane wyniki (TABELA 5, RYS.10) z wynikami badań zmęczeniowych „na sucho" (TABELA 4, RYS. 4) można zauważyć, że symulacja warunków pracy ma znaczący wpływ na wytrzymałość zmęczeniową płytek kompozytowych.

Analizując sposób niszczenia płytek kompozytowych stwierdzono, że pojawiające się pęknięcia przebiegały przede wszystkim w miejscach krytycznego przekroju (otworów), oraz występowały w różnych kierunkach, nawet wzdłuż podłużnej osi próbki. Pierwsze pęknięcia najczęściej pojawiały się po mniej niż 1000 cykli i prawie zawsze lokalizowały się w okolicach dalszego otworu (mierząc od środka na długości płytki), propagując na otwory bliższe. W przypadku płytek typu N pęknięcie niszczące najczęściej przebiegało poprzecznie przez jeden z otworów bliższych środka płytki (RYS. 11). Z kolei pęknięcia płytek R przebiegały głównie wzdłuż osi długiej płytki (RYS. 12).

The comparison of the obtained results (TABLE 5, FIG. 10) to the "dry" fatigue tests (TABLE 4, FIG. 4) proves that the working conditions significantly affect the fatigue strength of composite plates.

The analysis of the destroyed composite plates revealed that the cracks occurred mainly at the critical cross-section (holes), in various directions, even along the longitudinal axis of the sample. The first cracks most often appeared after less than 1,000 cycles and almost always they were located near the further hole (measured from the middle of the length of the plate), propagating to proximal holes. In the case of N-type plates, the destructive fracture usually ran transversely through one of the holes closer to the centre of the plate (FIG. 11). In turn, cracks in the R plates ran mainly along the long axis of the plate (FIG. 12).

TABELA 5. Wyniki próby cyklicznego rozciągania w symulowanym środowisku biologicznym.
TABLE 5. Results of the cyclic tensile strength tests in the simulated biological environment.

		Płytka / Plate PLA/TCP/HAp		
Wielkość odkształcenia - Amplituda ε_{Fmax} Cyclic deformation values (amplitude) used in fatigue tensile tests ε_{Fmax}		50%	40%	30%
Liczba cykli do pierwszego pęknięcia First crack cycle number	N	---	---	~250
	R	---	~250	~850
Liczba cykli przy których nastąpiło zniszczenie płytki Number of cycles for sample destruction	N	---	---	~2000
	R	---	~400	~5500

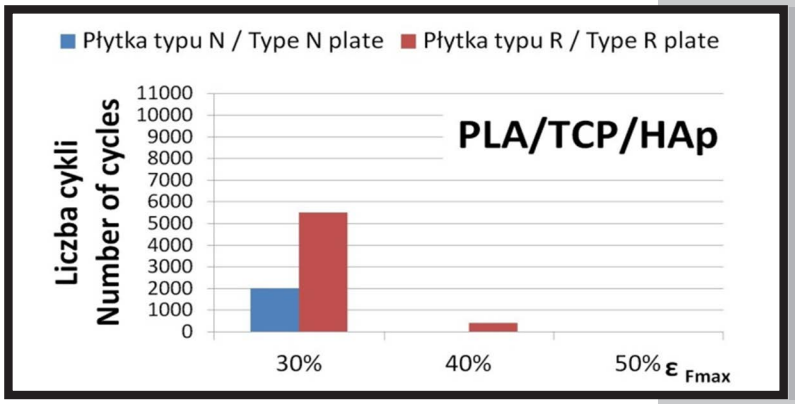

RYS. 10. Zestawienie wytrzymałości zmęczeniowej płytek czterootworowych w testach symulujących środowisko biologiczne.
FIG. 10. Comparison of fatigue strength of four-holes plate after testing in biological simulated conditions.

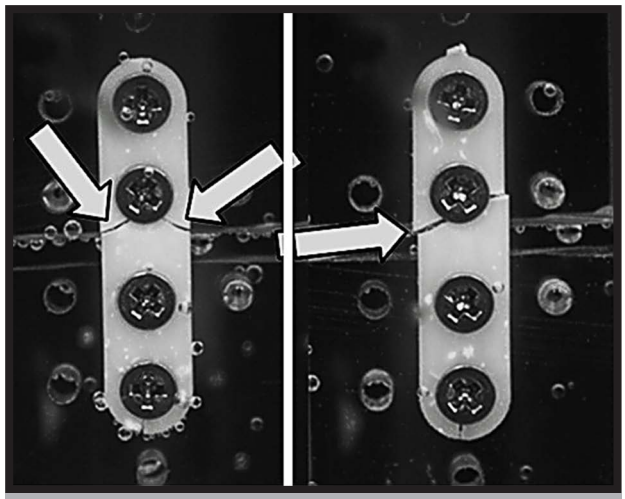

RYS. 11. Przykładowe pęknięcia kompozytowych płytek I typu N (PLA/TCP/HAp).
FIG. 11. Cracking nature of exemplary N-type plates (PLA/TCP/HAp).

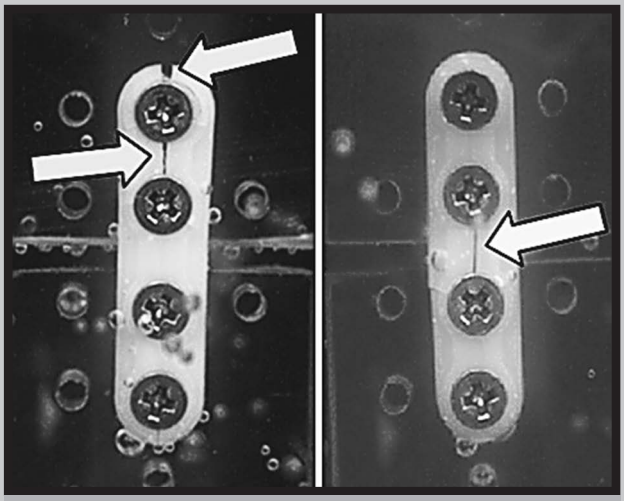

RYS. 12. Przykładowe pęknięcia kompozytowych płytek I typu R (PLA/TCP/HAp).
FIG. 12. Cracking nature of exemplary R-type plates (PLA/TCP/HAp).

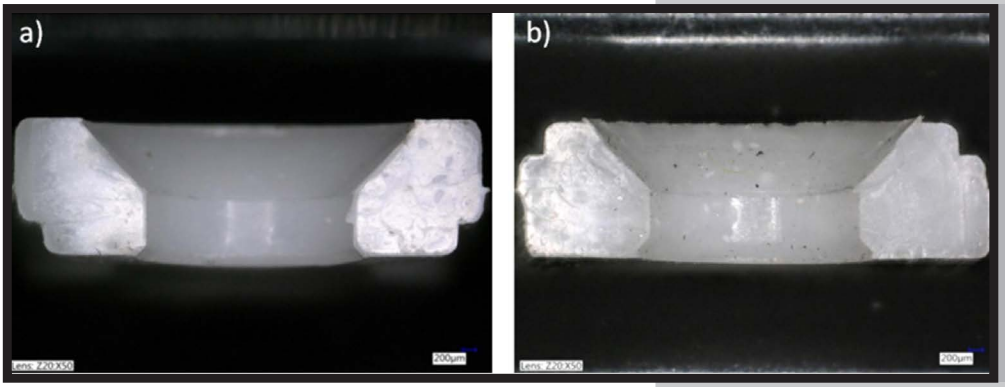

RYS. 13. Przekroje krytyczne:
a) płytka typu N;
b) płytka typu R (x50).
FIG. 13. Critical cross--section of plates:
a) N-type;
b) R-type (x50).

Taki przebieg linii pęknięć może być związany z geometrią płytek tj. lokalizacją żeberka wzmacniającego. Ono może powodować zmiany w rozkładzie naprężeń, ponieważ pole przekroju krytycznego w obu przypadkach jest inne (RYS. 13). Wskazanie przyczyny takiego zachowania się płytek wymaga przeprowadzenia dalszych badań ukierunkowanych na szczegółową analizę naprężeniowo-odkształceniową w obszarach otworów mocujących.

Podsumowanie

Prezentowany artykuł przedstawia wyniki wstępnych badań przeprowadzonych na ograniczonej liczbie próbek. Z tego powodu nie zamieszczono analiz statystycznych i odchyleń standardowych wyznaczanych parametrów. Dlatego zawarte informacje powinny być traktowane jako opis pierwszych spostrzeżeń, które pojawiły się podczas testów mechanicznych symulujących warunki pracy implantów. Przeprowadzone badania zmęczeniowe, a zwłaszcza te które odwzorowywały warunki pracy implantów pokazały, że środowisko biologiczne ma znaczący wpływ na zachowanie się i charakterystyki implantów. Testowane płytki do zespoleń kostnych wykonane z kompozytu PLA/TCP/HAp badane „na sucho" były w stanie pracować przez krótki czas nawet przy obciążeniach sięgających 50% ε_{Fmax}. Po umieszczeniu ich w symulowanym środowisku biologicznym były w stanie pracować bezpiecznie, przetrwać bez zniszczenia 10000 cykli, ale przy amplitudzie zredukowanej do 30% ε_{Fmax}. Analizując wpływ ogrzanego sztucznego płynu fizjologicznego na badane próbki stwierdzono, że nie dochodziło do termicznego uplastycznienia płytek, gdyż ich uszkodzenia miały zawsze charakter kruchego pęknięcia. Zatem temperatura 37°C, w jakiej prowadzono testy symulacyjne (temperatura płynu) jest zbyt niska, aby zapoczątkować jakiekolwiek zmiany strukturalne.

Podczas obserwacji i analizy przełomów zniszczonych płytek stwierdzono, że bardzo często miejscem inicjacji uszkodzeń były widoczne makroskopowo aglomeraty proszku TCP/HAp, które mogły być punktami koncentracji naprężeń. W związku z tym wnioskuje się, aby podczas procesu wytwarzania metodą wtrysku kłaść duży nacisk na odpowiednią homogenizację wsadu. Dzięki temu uzyskana wypraska powinna posiadać bardziej jednorodną strukturę, a równomierny rozkład cząstek będzie utrudniał rozchodzenie się pęknięć, zwiększając tym samym wytrzymałość implantu oraz odporność na zniszczenie zmęczeniowe.

Kolejnym spostrzeżeniem jest to, że geometria płytki, a dokładniej umiejscowienie żeberka wzmacniającego, ma duży wpływ na wytrzymałość zmęczeniową oraz przebieg linii pękania. Płytka typu R cechowała się trzykrotnie wyższą trwałością niż płytka typu N. Co ciekawe, podobnej zależności nie stwierdzono podczas prób statycznego jednoosiowego rozciągania (poprzedzającej badania zmęczeniowe), gdzie dla obu wariantów geometrycznych płytek (N i R) uzyskano zbliżone wartości parametrów mechanicznych.

Such a line of cracks can be associated with the geometry of the plates, i.e. the location of the reinforcing rib. The rib may alter the stress distribution, as the critical cross-sectional area is different in both cases (FIG. 13). To discover and to describe the behaviour of the plates under cyclic stretching, specially cracks propagation, additional analyses focused on stress and deformation characteristics in conical holes surroundings, need to be conducted.

Conclusions

The article presents preliminary research thus the number of samples was limited. The results do not include statistical analysis and standard deviations thus they should be treated as the first remarks. The conducted fatigue tensile strength tests, especially those mimicking the working conditions of the implants, proved that the biological environment significantly affects the behaviour and characteristics of the implants. The PLA/TCP/HAp composite plates tested in "dry" conditions were able to work for a short time even at loads up to 50% ε_{Fmax}. However, when placed in the simulated biological environment only the amplitude reduced to 30% ε_{Fmax} guaranteed proper functioning and the samples survived 10,000 cycles without destruction. Analyzing the effect of heated artificial physiological fluid on the tested samples, it was found that no thermal plasticizing of the plates took place – the fracture was always a brittle one. The conclusion is that the temperature of 37°C is too low to initiate any structural changes.

During the observation and analysis of the fractures of damaged plates, it was found that very often the cracks occurred due to the macroscopically visible powder agglomerates of TCP/HAp which could be the points of strain concentration. Therefore, it is crucial to place a high emphasis on adequate homogenization of the material during the injection moulding process to ensure that the obtained plates are perfectly homogeneous structures. An even distribution of particles will hinder the propagation of cracks, thereby increasing the strength of the implant and resistance to fatigue failure.

Another observation is that the geometry of the plate, and more precisely the location of the reinforcing rib, has a large impact on fatigue strength and the direction of the crack. The R plate fatigue resistance was three times longer than the N-type plate. Interestingly, a similar relationship was not found during static uniaxial stretching tests (preceding fatigue tests), where both geometric variants of the plates (N and R) revealed similar mechanical parameters.

Przeprowadzone testy udowodniły, że symulowane warunki pracy w przypadku implantów kompozytowych mają znaczący wpływ na zmiany ich charakterystyk mechanicznych, a zwłaszcza odporności na działanie obciążeń cyklicznie zmiennych w czasie. Wynika z tego, że każdy prototypowy implant powinien być badany w taki sposób, aby schemat badań laboratoryjnych w jak największym stopniu odwzorowywał rzeczywiste warunki pracy. Dopiero po przeprowadzeniu takich testów, weryfikacji i analizie wyników można zdecydować czy implant spełnia warunki projektowe.

Podziękowania

Badania wykonano przy współpracy z firmą MEDGAL Białystok, w ramach projektu badawczo-rozwojowego: „Opracowanie i wdrożenie technologii produkcji innowacyjnych implantów kostnych z kompozytów polimerowych" (POIG 01.04.00-20-003/10). Autorzy pragną również podziękować: Mai Kuś, Natalii Kosibie oraz Grzegorzowi Janiszewskiemu, za pomoc przy realizacji badań.

The results of the conducted tests prove that simulated working conditions have a significant impact on the mechanical characteristics of composite implants, in particular, the resistance to cyclically changing loads. Therefore, each prototype implant should be tested in the environment mimicking the real working conditions as much as possible. Only such thorough tests, followed by further verification and analysis of the results will prove that the implant is safe and meets the designed requirements.

Acknowledgments

The research was carried out in cooperation with MEDGAL Bialystok, as part of a research and development project: "Development and implementation of production technology for innovative bone implants made of polymer composites" (POIG 01.04.00-20-003 / 10). The authors would also like to thank: Maja Kuś, Natalia Kosiba and Grzegorz Janiszewski for their help in carrying out the research.

References

[1] Ho-Yong Lim, Chang-Hwa Jung, Seong-Yong Kim, Jin-Yong Cho, Jae-Young Ryu, Hyeon-Min Kim: Comparison of resorbable plates and titanium plates for fixation stability of combined mandibular symphysis and angle fractures. J Korean Assoc Oral Maxillofac Surg 40 (2014) 285-290.
[2] G. Harsha, S. Ganesh Kumar Reddy, Sunil Talasila, S. Abdus Salaam, M. Srinivasulu, V. Sridhar Reddy: Mandibular Reconstruction using AO/ASIF Stainless SteelReconstruction Plate: A Retrospective Study of 36 Cases. The Journal of Contemporary Dental Practice 13(1) (2012) 75-79.
[3] Lop Keung Chow, Lim Kwong Cheung, Wei Ren: Resorbable Plate Fixation for Maxillofacial Fractures and Osteotomies. Asian J. Oral Maxillofacial Surgery 16(4) (2004) 224-233.
[4] Takahiro Kanno, Shintaro Sukegawa, Yoshihiko Furuki, Yoshiki Narai, Joji Sekine: Overview of innovative advances in bioresorbable plate systems for oral and maxillofacial surgery. Japanese Dental Science Review 54 (2018) 127-138.
[5] Błażewicz Stanisław, Marciniak Jan i wsp.: Inżynieria biomedyczna - Podstawy i zastosowania. Tom 4 – Biomateriały. Akademicka oficyna wydawnicza EXIT, ISBN 978-83-7837-054-3 (2016)
[6] Conte R., Di Salle A., Riccitiello F., Petillo O., Peluso G., Calarco A.: Biodegradable polymers in dental tissue engineering and regeneration. AIMS Materials Science 5(6) (2018) 1073-1101.
[7] Maurus P.B., Kaeding C.C.: Bioabsorbable Implant Material Review. Oper Tech Sports Med 12 (2004) 158-160.
[8] Kontakis G.M., Pagkalos J.E., Tosounidis T.I, Melissas J., Katonis P.: Bioabsorbable materials in orthopaedics. Acta Orthop. Belg. 73(2) (2007) 159-169.
[9] Alizdeh-Osogouei M., Yuncang Li, Cuie Wen: A comprehensive review of biodegradable synthetic polymer-ceramic composites and their manufacture for biomedical applications. Bioactive Materials 4(1) (2019) 22-36. [10] Moser R.C., McManus A.J., Riley S.L., Thomas K.A.: Strength Retention of 70:30 Poly(L-Lactide-co-D,L-Lactide). Following Real-Time Aging. J Biomed Mater Res B Appl Biomater. 75(1) (2005) 56-63.
[11] Rishi K. Bali, Sharma Parveen, Jindal Shalu, Gaba Shivani: To evaluate the efficacy of biodegradable plating system for fixation of maxillofacial fractures: A prospective study. National Journal of Maxillofacial Surgery 4(2) (2013) 167-172.
[12] Yuehuei H., Draughn R.A.: Machanical Testing of Bone and the Bone-Implant Interface. CRC Press LLC 2000, ISBN 0-8493-0266-8
[13] Shikinami Y., Okuno M.: Bioresorbable devices made of forged composites of hydroxyapatite (HA) particles and poly l-lactide (PLLA). Part II: practical properties of miniscrews and miniplates. Biomaterials 22 (2001) 3197-3211.
[14] Karpiński R., Jaworski Ł., Czubacka P.: The structural and mechanical properties of the bone. Journal of Technology and Exploitation in Mechanical Engineering 3(1) (2017) 43-50.
[15] Gryń K., Szaraniec B., Morawska-Chochół A., Chłopek J.: Charakterystyka mechaniczna wielofunkcyjnej resorbowalnej płytki kompozytowej do zespoleń kostnych / Mechanical characterization of multifunctional resorbable composite plate for osteosynthesis. Engineering of Biomaterials 133 (2015) 22-33.
[16] Norma PN-EN ISO 527-1:2012: Tworzywa sztuczne - Oznaczanie właściwości mechanicznych przy statycznym rozciąganiu - Część 1: Zasady ogólne.